Thesis for the degree of Doctor of Philosophy

CFD Modeling of an Alcohol-Diesel Direct-Injection Dual-Liquid-Fuel Engine using OpenFOAM

Andreas Nygren

Department of Mechanics and Maritime Sciences
CHALMERS UNIVERSITY OF TECHNOLOGY
Göteborg, Sweden 2021

CFD Modeling of an Alcohol-Diesel Direct-Injection Dual-Liquid-Fuel Engine using OpenFOAM
Andreas Nygren
ISBN 978-91-7905-461-8

Doktorsavhandlingar vid Chalmers tekniska högskola
Ny serie nr 4928
ISSN 0346-718X

Department of Mechanics and Maritime Sciences
Chalmers University of Technology
SE–412 96 Göteborg, Sweden
Telephone + 46 (0) 31 – 772 1000

Cover: Stoichiometric surface of Methanol colored by temperature.

Typeset by the author using LaTeX.

Printed by Chalmers Reproservice
Göteborg, Sweden 2021

Abstract

Legislation for heavy duty combustion engines are becoming more stringent. To keep up with the legislation, new engine technology is required. Furthermore, renewable fuels can also be used together with new engine technology to further reduce emissions.

Computational techniques such as Computational Fluid Dynamics (CFD) provides a powerful and cost effective alternative/complement to traditional engine tests when developing new engine technology. To effectively use CFD for engine development, accurate models for spray formation and chemistry are required. In this work a new direct-injection dual-liquid-fuel engine concept using methanol and diesel was investigated using CFD. The first part of this thesis involved validation and development of our in-house spray model, VSB2. The VSB2 is a Eulerian-Lagrangian model with a minimal amount of tuning parameter. It models the impact of secondary breakup by including a distribution of droplet sizes inside each computational blob. The model was first validated for use with alcohol fuels, where the turbulence parameters were also tuned together with experimental data for later use in engine simulations. It was shown that the VSB2 spray model could accurately predict the spray formation of an alcohol spray.

Furthermore, the spray model was developed further by implementing a new break up treatment that addressed some conceptual flaws in how the model handles the momentum of a computational blob with different droplet sizes. Previously, each computational blob contained the momentum of all droplet sizes, which had the consequence that smaller droplets would have the same momentum as larger droplets. This was addressed by creating child blobs from the stable droplet sizes. It was shown that this had the effect of enhancing the evaporation and dispersion at lower ambient gas temperatures.

The last part of this thesis was to create a CFD model in OpenFOAM that could model a direct-injection dual-liquid-fuel engine. A tabulated chemistry solver based on the well stirred reactor approach called LOGE-CPV was used to model the chemistry. It was shown that the model could accurately predict global parameters such as in cylinder pressure and rate of heat release of the system, but pollutant formation was predicted poorly when compared to experiments. It was concluded that a turbulent combustion model would be needed to accurately predict pollutant formation. The ignition process was also studied, showing that the pilot diesel could easily ignite the methanol as long as the pilot flame would reach the center of the combustion chamber. It was also shown that further offsetting the pilot injector caused the combustion to become unstable as it was difficult to ignite all the sprays from the main injector. **Keywords: CFD, Dual-Fuel Combustion, Spray Modeling, Renewable Fuels**

Acknowledgments

First of all I would like to thank and acknowledge my supervisor Anders Karlsson and my former manager Ingemar Denbratt for giving me the opportunity to work at Chalmers. It has been some really great years at Chalmers, and I can hardly believe how fast it all went. Thanks to the both of you for hiring me, it has been really great working with you.

I would also like to thank all the people in the F-Flex project team from Volvo AB and LOGE. It was great working with all of you.

The greatest acknowledgement goes to all the people at the Division of Combustion and Propulsion Systems. Thank you for all the great after-work beers, and all the fun times we have had together. A very special thank you goes to Michael Saccullo and Vignesh Pandian Muthuramalingam, who I spent most of my time together with in our office. Without the two of you, going to work would not have been nearly as fun.

Finally, I would like to thank my family for all their support during this time.

Funding from the Swedish Energy Agency is gratefully acknowledged.
Andreas Nygren
Göteborg, March 2021

List of Publications

This thesis is based on the following appended papers:

Paper 1. Andreas Nygren and Anders Karlsson. *Validation of the VSB2 Spray Model for Ethanol under Diesel like Conditions.* SAE Technical Papers 2017-01-2193, 2017

Paper 2. Andreas Nygren and Anders Karlsson. *A study of ECN spray A using an improved stochastic blob (VSB2) spray model.* Proceedings of 14th International Conference on Liquid Atomization and Spray Systems (ICLASS), Chicago, USA, 2018.

Paper 3. Vignesh Pandian Muthuramalingam, Andreas Nygren and Anders Karlsson. *A comprehensive study on the influence of resolving an injector orifice and the influence of creating stripped off droplets on spray formation using the VSB2 spray model.* Accepted for publication in Atomization and Sprays.

Paper 4. Michael Saccullo, Andreas Nygren, Timothy Benham and Ingemar Denbratt. *Alcohol flexible HD Single Cylinder Diesel Engine Tests with Separate Dual High Pressure Direct Fuel Injection.* Accepted for publication in Fuel.

Paper 5. Andreas Nygren, Michael Saccullo and Anders Karlsson. *CFD Modeling of a Direct Injection Dual Fuel Engine.* Submitted for publication to the International Journal of Engine Research.

Other relevant publications co-authored by Andreas Nygren:

Paper 6. Tim Lackmann, Andreas Nygren, Anders Karlsson and Michael Oevermann. *Investigation of turbulence–chemistry interactions in a heavy-duty diesel engine with a representative interactive linear eddy model .* International Journal of Engine Research. 2020;21(8):1469-1479.

Paper 7. Magnus Walander, Andreas Nygren, Jonas Sjöblom, Emil Johansson, Derek Creaser, Jonas Edvardsson, Stefanie Tamm, and Björn Lundberg. *Use of 3D-printed mixers in laboratory reactor design for modelling of heterogeneous catalytic converters .* Accepted for publication in Chemical Engineering and Processing: Process Intensification.

Contents

Part I

Introductory chapters

Chapter 1

Introduction

1.1 Motivation & Background

The world is ever evolving, and global demands for the transportation of goods is increasing due to a growing world economy and population. The transportation of goods can typically be divided into three types

1. Road Freight
2. Rail Freight
3. Maritime Freight

Road freight is the most flexible of the above-listed modes of transportation since it does not require a rail network or ocean shipping lanes to be available. However, it is also the least energy efficient. Road freight transport only accounts for 20 % of the global transport kilometers but consumes more than 70 % of the energy used in freight transportation [39]. The European Commission estimated in the 2016 reference scenario that demand for the transportation of goods by road freight would increase by 57 % by 2050 [6]. Increased demand for transportation with conventional trucks will inevitably lead to increased greenhouse gas (GHG) emissions. Many of the world's countries have agreed to the Paris Climate Agreement, which aims to limit global warming to below 2 °C by reducing CO2 emissions [61]. However, global CO2 emissions from trucks steadily increased between 2000 and 2018 according to data from the International Energy Agency (IEA) (Figure 1.1) [18]. To adhere to the Paris Agreement, CO2 emissions should be decreased according to the "Sustainable Development Scenario" (SDS) presented by the IEA [19]. Adherence to the SDS is represented by the projected data between 2018-2030 in Figure 1.1.

GHG emissions are not the only issue arising from increased demands for road freight transportation. Due to the superior efficiency of diesel engines, almost all trucks are fueled by diesel. This gives rise to local, harmful emissions, such as NOx, carbon monoxide (CO), unburned hydrocarbons (HC) and soot. It has been shown that increased concentrations of pollutants in the air correlate with increased mortality and hospitalization [23].

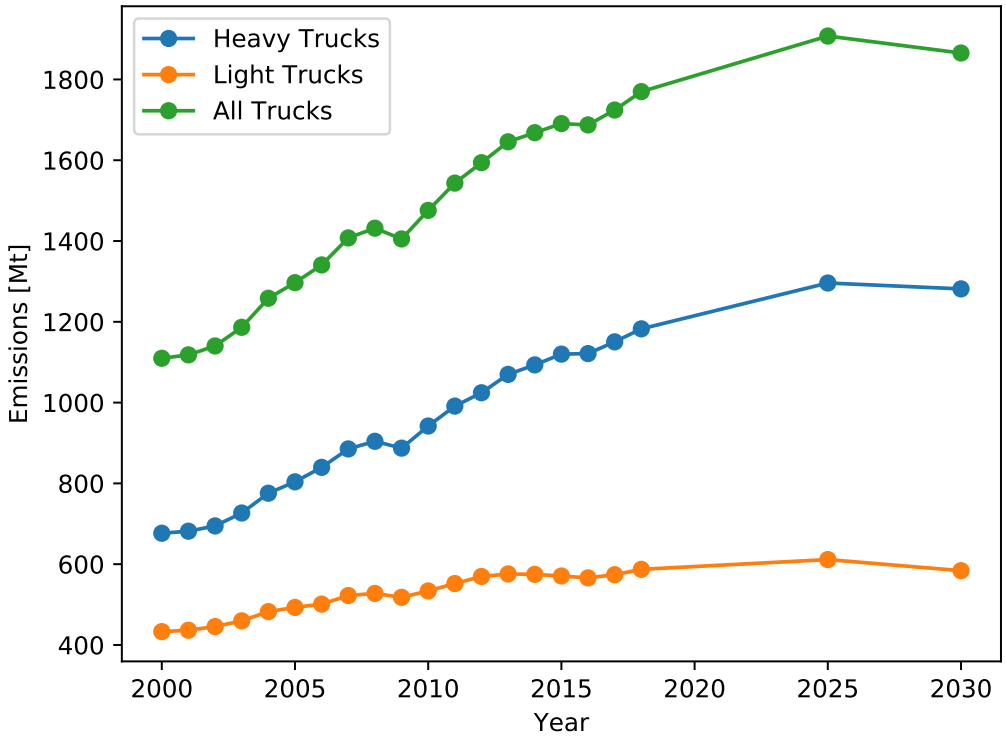

Figure 1.1: Globally measured CO_2 from light and heavy trucks. Data after 2018 is a projection based on SDS. [18]

Clearly, there is a need for a reduction in both GHG and harmful emissions to reach the targets of the Paris Agreement. However, this is likely to be difficult if the current trend of increasing demands for transportation and energy continues. To achieve lower emissions while keeping up with the increased demand for transportation, new technology is required that increases the efficiency of transportation with respect to GHG emissions. Large-scale problems such as global warming are excellent drivers for the development of new technology. During the last few decades, the efficiency of diesel engines has been improved greatly, and in combination with exhaust aftertreatment, emissions have been greatly reduced. However, to reach the current targets, even further development is required, such as the introduction of renewable fuels in combination with new engine technology. Alcohol fuels that are produced from renewable sources offers an attractive alternative to the fossil based fuels that are commonly used today. Especially if a well-to-wheel approach is considered. Investigations with alcohol fuels such as methanol and ethanol have yield promising results with high efficiencies and low soot emissions due to the oxygen present in the fuel molecule. An issue with methanol an ethanol are that they can be difficult to compression ignite due to a low cetane number. In a situation where a fuel is difficult to ignite, but have other attractive properties, dual-fuel combustion is an alternative. Such a combustion system allows for the introduction of a small

amount of easily ignitable fuel to help ignite the main fuel.

1.2 Research Questions and Objectives

In the work upon which this thesis is based, a direct-injection dual-fuel engine configuration was studied using computational fluid dynamics (CFD). CFD has emerged in recent years as a powerful tool to develop new engine technologies. It can be a cost- and time-effective complement to engine testing and can provide detailed information to engine researchers that is not obtainable by conventional engine testing.

The engine studied in this work used methanol as a main fuel and diesel as a pilot. Both fuels were directly injected into the engine. The combustion strategy of the engine was similar to that of a conventional diesel engine with a late fuel injection close to top dead center (TDC).

The overall aim of this project was to investigate and demonstrate technical solutions that can be applied to a future fuel flexible powertrain solution. The main goals of the project can be summarized as follows:

- Achieve a higher efficiency than a conventional Diesel engine, i.e., greater than 48 %.
- Achieve a reduction of GHG emissions by 90 % or more by using renewable fuels in a well-to wheel approach.
- Satisfy the EURO VI emissions legislation with minimal fuel penalty caused by exhaust gas recirculation (EGR).

To study this system, both CFD simulations and single-cylinder experiments were conducted, with the CFD studies being the focus of this thesis. To study a direct injection engine, it is important that spray formation is accurately predicted. The first part of this work was to study and validate the use of a previously developed in-house spray model (VSB2) for use with an ethanol spray. This was carried out by simulating an ethanol spray in the Chalmers high-pressure/high-temperature spray chamber under diesel-engine-like conditions and comparing the predicted spray penetration with experimentally measured values. The results of the spray study were used to tune the turbulence parameters used for all further studies with alcohol sprays. The second part of this work was to extend the VSB2 spray models breakup formulation to better account for the formation of stripped off droplets. To validate the new breakup treatment, the new and old breakup treatments were compared with experimental data from the Engine Combustion Network (ECN). The final part of this work consisted of using the validated and improved spray model to create a CFD model of a direct-injection dual-fuel engine. The simulated pressure, heat release and emissions were then compared with experiments. The objectives of the work described in this thesis can be summarized in the following research questions:

- **What is the influence of creating new child parcels from the stable droplets in the VSB2 spray model?** Previously, the VSB2 model has

modeled the impact of secondary breakup by defining a distribution function describing the distribution of droplet sizes inside each computational blob. A downside of this approach is that droplets of all sizes in a computational blob will travel with the same momentum. A more accurate approach would be to create new child blobs for the stable droplet.

- **Is it possible to model the formation of an alcohol spray using the VSB2 spray model without any conceptual changes to the model?** The VSB2 model has previously been designed and validated for diesel sprays using a high pressure injection. Lower alcohol fuels are typically used in light duty, spark ignited engines with a lower injection pressure. Therefore, it would be of interest to investigate how predictive the model is for an alcohol spray.
- **What does the combustion process look like inside a direct-injection dual-fuel engine?** A direct-injection dual- fuel engine with liquid fuels is a novel concept and the combustion process should be studied
- **Can we model the combustion process inside a direct-injection dual-fuel engine using a simplified model that does not account for turbulence-chemistry interactions?** Many established models for non-premixed turbulent combustion are unsuitable for dual-fuel combustion. For this reason, the well stirred reactor (WSR) approach was chosen for this work. However, the approach needs to be validated by comparing with experimental data.

1.3 Organization of this Thesis

This thesis is organized into seven different chapters, which are summarized below:

- **Chapter 1** explains the motivation for this work and the objectives.
- **Chapter 2** contains a literature review of the subjects relevant to this study, i.e., sprays, combustion modeling and engine technologies
- **Chapter 3** presents the approach used to model the gas phase.
- **Chapter 4** presents the VSB2 spray model that was used to model the liquid phase.
- **Chapter 5** Summarizes the main results and findings.
- **Chapter 6** Presents conclusions and suggestions for further studies.

Chapter 2

Engine, Spray and Turbulent Combustion Fundamentals

2.1 Compression Ignited Engines

Compression ignited (CI) conventional diesel engines make up the vast majority of trucks used for road transportation. Conventional diesel engines have long suffered from the well-known "diesel dilemma", also known as the soot-NO_x trade-off. Soot tends to form in fuel-rich areas that are present due to the nature of the non-premixed combustion occurring inside diesel engines [11]. At low equivalence ratios close to 1, the temperatures tend to be higher, resulting in higher NO_x according to the well-known Zeldovich mechanism [65]. New technologies for CI engines are attempting to address the soot-NO_x trade-off by lowering the combustion temperature to achieve low temperature combustion (LTC), using alternative fuels or a combination of both approaches.

2.1.1 Dual Fuel Combustion

Dual-fuel combustion is a term applied to a combustion process where instead of one fuel, two fuels are burned inside the combustion chamber. A dual-fuel system can be used to construct advanced combustion modes, where one fuel is used to compensate for the poor reactivity of another fuel that may otherwise have desirable properties. Several dual-fuel combustion systems have been proposed in the literature. For example, a port-fuel injected system with reactivity controlled compression ignition (RCCI) has been proposed by Kokjohn et al. [27]. In RCCI, the combustion is optimized by controlling the reactivity of the combusting mixture. The main fuel is port injected and is allowed to mix with the incoming air. The reactivity is controlled by directly injecting diesel into the combustion chamber in an appropriate way for the desired speed/load point until the mixture auto-ignites. RCCI has been shown to allow increased control compared to other early injection CI systems, such as HCCI [52]. Another technique for dual-fuel combustion is direct-injection dual-fuel combustion. This refers to direct injection of both high and low cetane number fuels into the cylinder. This is the type of system studied in the present work, and only a

few studies have so far examined this strategy. A concept similar to the one used in this work was studied by Ullman et al. [60] who utilized methanol as the main fuel and diesel as the pilot with promising results. A more recent numerical study was conducted by Giramondi et al. [15] on an ethanol-diesel system. They showed that ethanol auto-ignited at high loads with a high degree of premixture and that it was necessary to advance the start of injection of the diesel pilot to achieve diffusive combustion.

2.2 Sprays

A spray can be described as a collection of many liquid droplets dispersed in a gas. It is an important process in many industrial applications, such as manufacturing, food, power and especially the automotive industry in the form of fuel sprays. Typically, fuel is injected either directly into the cylinder or in the intake port. This section describes the fundamentals of spray formation and reviews commonly used approaches to model sprays.

2.2.1 Spray Formation and Break up

When a liquid is injected at a high velocity relative to its surroundings, a jet will form and start to break up. This process is commonly referred to as primary breakup. In primary breakup, four different regimes are usually identified depending on the Ohnesorge and liquid Weber numbers: the Rayleigh regime, the first and second wind regimes and the atomization regime[1]. For high pressure injections such as in diesel engines, the atomization regime is the most relevant. Figure 2.1 shows a schematic overview of typical spray breakup in the atomization regime. The primary breakup causes the liquid jet to split up into ligaments almost immediately, and a small conically shaped liquid core is retained close to the nozzle. The physics of primary breakup are difficult to study under engine-like conditions due to the high optical densities and high velocities in the near nozzle region. Several studies have evaluated different experimental techniques[10, 33, 32], but the primary breakup process is still poorly understood.

Due to the large drag forces created by the high relative velocity, the spray will break up further into small droplets. This is referred to as secondary breakup. In secondary breakup, several regimes can be identified based on the gas-phase Weber number:

$$\mathrm{We}_g = \frac{\rho_g u_{\mathrm{Rel}}^2 d}{\sigma} \tag{2.1}$$

where ρ_g is the gas density, u_{rel} is the relative velocity, d is the droplet diameter before breakup and σ is the surface tension. The Weber number describes the ratio of drag forces to surface forces acting on a droplet. If the drag forces are large relative to the surface tension, the droplets tend to break up into small more stable droplets. In an engine, these small droplets tend to evaporate quickly due to the high ambient temperature.

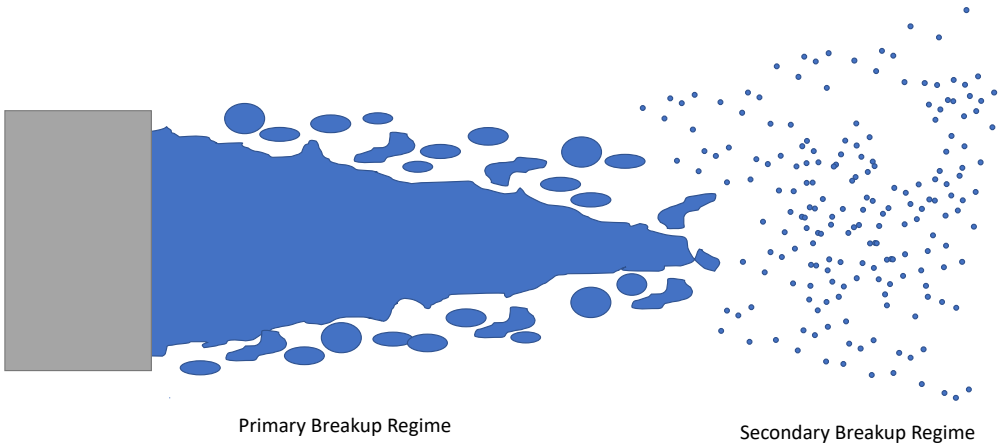

Figure 2.1: Schematic overview of the spray breakup process.

2.2.2 Modeling of Sprays

The spray formation governs the mixing inside an engine. Thus, for accurate modeling, prediction of the spray formation is very important. A spray is also an example of a multi-phase system, where the spray droplets are considered the dispersed phase and the surrounding gas considered as the continuous phase. Several approaches have been proposed to model multi-phase systems in CFD. Commonly, they are classed as either interface resolving methods or non-interface resolving methods. The volume of fluid method is one of the most common interface tracking methods implemented in commercial CFD codes. It was first proposed by Hirt and Nichols [16] and involves tracking the interface between the continuous and dispersed phase. The volume fraction α is defined as $\alpha = 0$ for a pure continuous phase and $\alpha = 0$ for a pure dispersed phase. A value between 0 and 1 indicates that there is an interface. To track the interface, a transport equation for α is formulated:

$$\frac{\partial \alpha}{\partial t} + \nabla \cdot \mathbf{u}\alpha = S_\alpha \tag{2.2}$$

Note that while this approach can yield a very accurate prediction of a gas-liquid multi-phase system, the method may be unsuitable for dense sprays due to the computational requirements. In particular, the computational grid has to be fine enough to capture the interface for many small droplets. For engine simulations, the volume of fluid method has often been applied to the in-nozzle flow of an injector [54, 41]. The results of the in-nozzle simulation can then be used as a size distribution for an in-cylinder simulation to account for primary breakup. Another approach to multi-phase flow is the two-fluid approach originally proposed by Ishii and Mishima [20]. The two-fluid model is a Eulerian-Eulerian type model where both phases are treated in an Eulerian frame of reference. Both phases are regarded as a continuum

described by the Navier-Stokes equation. The model does not resolve any interface between phases but instead calculates the volume fraction of each phase inside a grid cell. Coupling between the phases is achieved using source terms. This approach has been successfully applied to model diesel sprays[21].

The most common approach to model sprays in engines is the Eulerian-Lagrangian approach. In this approach, the continuous phase is governed by the Navier-Stokes equation and the dispersed phase is treated in a Lagrangian frame of reference as particles governed by Newtonian mechanics. Each particle represents a collection of droplets, and submodels are applied on each particle to account for physical processes, such as primary and secondary breakup, evaporation and heat transfer. Primary breakup governs the initial particle sizes in the Eulerian-Lagrangian approach. For high pressure sprays in the atomization regime, Reitz and Diwakar [51] proposed that the near nozzle breakup and atomization are indistinguishable processes. Therefore, a detailed primary breakup model can be replaced by a simple "blob injection" method, where the injected particles have the same diameter as the injector nozzle. This will form large particles in the area around the nozzle, mimicking the formation of a liquid core that is typically seen for sprays in the atomization regime. Secondary breakup is normally treated in more detailed engine simulations. Several models based on physical phenomena are available, such as the Taylor-analogy-breakup (TAB) model proposed by O'Rourke and Amsden [40]. This model is based on the Taylor analogy between oscillating and distorting droplets and a spring mass system. Other physical models include the Kelvin-Helmholtz model proposed by Reitz [50], also known as the WAVE model. This model is based on an analysis of the well-known Kelvin-Helmholtz instability and assumes that the time of breakup is related to the fastest growing Kelvin-Helmholtz instability. The wavelength and growth rate of the instability can be used to predict details of newly formed droplets. The Kelvin-Helmholtz model is often used together with the Rayleigh-Taylor model to improve breakup prediction close to the nozzle [1]. The breakup rate correlation proposed by Pilch and Erdman [44] is an example of a phenomenological model proposed by fitting data to experiments. This model is discussed further in Chapter 4. The Eulerian-Lagrangian approach has been successfully applied by many authors to model spray formation and combustion [42, 17, 36, 25, 22, 2, 48].

2.3 Combustion

Combustion is a chemical process where fuel reacts with an oxidizer, typically oxygen. Combustion products are formed and energy is released. An example of a combustion reaction equation for a general hydrocarbon fuel F is

$$\mathrm{F} + a\mathrm{O}_2 \longrightarrow b\mathrm{CO}_2 + c\mathrm{H}_2\mathrm{O}$$

Combustion is an example of an exothermic process, where chemical energy stored in the fuel is converted into heat. This heat can then be converted into useful work in a combustion engine. Combustion engines can be divided based on two different modes: premixed and non-premixed combustion. Intermediate modes, such

as partially premixed combustion, are also possible. Premixed combustion refers to a mode where the fuel and oxidizer are completely mixed before ignition, whereas non-premixed combustion, also known as diffusion-controlled combustion, refers to a mode where the fuel and oxidizer are separated and the combustion rate is controlled by the mixing of fuel and oxidizer. The scope of this thesis is limited to non-premixed combustion.

2.3.1 Turbulent Combustion

Many models have been proposed in the literature to model turbulent non-premixed combustion together with finite rate chemistry. Turbulent non-premixed flames are characterized by a thin reaction zone where a stoichiometric mixture is present. Turbulence affects the reaction zone by wrinkling it. The main challenge in modeling turbulent combustion in CFD is to include the effect of turbulence-chemistry interactions on the flame without resolving the turbulent fluctuations in the flame. The simplest approach is to directly compute the chemical source terms based on resolved mean values of species and temperature. This is commonly referred to as the well stirred reactor model (WSR). This approach completely ignores the effects of turbulence chemistry interactions but is commonly used for combustion simulations due to its simplicity and flexibility with respect to the chemical mechanism and composition of the fuel [55, 7, 64].

The partially stirred reactor model (PaSR) was proposed by Chomiak [4] as an extension of the WSR concept where each computational cell is split into two parts: one part where the reaction takes place and another part where only mixing occurs. The model was used to study flame lift-off in diesel sprays by Chomiak and Karlsson [5], and their results showed good agreement with theoretical data. D'Errico et al. [8] used the PaSR model to study combustion inside an optical engine. They showed that the model over-predicted the ignition delay compared to experiments.

A more common approach to model turbulent combustion under non-premixed conditions is the flamelet approach developed by Peters [43]. The steady flamelet model allows for decoupling of the chemistry and flow field, and the chemistry only needs to be solved in the mixture fraction space. A parameter known as the scalar dissipation rate is used to couple the flow to the chemistry. Since the chemical calculations are completely decoupled from the flow, they can be performed in a pre-processing step and stored in a library, which eliminates the need to solve transport equations and chemistry on-line, speeding up the calculations. To calculate the mean values, it is necessary to know the probability density function (PDF) of the mixture fraction. In the flamelet approach, it is commonly assumed that turbulent fluctuations follow a β distribution. The flamelet concept has also been used in a transient way, where the flamelet equations are solved online for better prediction of slow processes, such as NO_x formation [45]. D'Errico et al. [9] compared an unsteady flamelet model with the WSR approach. It was concluded that the flamelet model was better than the WSR approach for cases where the combustion is mixing controlled, such as conventional diesel combustion A limiting factor of the flamelet approach is that it is difficult to model more than one fuel.

Several models have been proposed in the literature that are mode and regime independent. One example is the transported PDF model proposed by Pope [46]. It has been successfully used to model turbulent combustion in spray bombs [2] and a heavy duty diesel engine [48]. The importance of accounting for turbulence-chemistry interactions for the accurate prediction of global parameters, such as the pressure and rate of heat release, and emissions was demonstrated. The transported PDF method is very computationally expensive and is best suited when a simple chemical mechanism with few species can be used. The linear eddy model (LEM) proposed by Kerstein Kerstein [26] is an example of a regime independent model that resolves the turbulent advection on a one-dimensional line, where a "triplet map" is used to emulate the effect of turbulent eddies on a one-dimensional line. The LEM has been used both as a subgrid model for large eddy simulations [57] and in RANS simulations [30].

Taken together, these studies illustrate the importance of properly including turbulence-chemistry interactions when modeling non-premixed combustion in CFD. Nevertheless, the WSR approach was chosen for the present work due to its simplicity and flexibility for modeling a dual-fuel system.

Chapter 3

Gas Phase Modeling

This chapter will present the approach used to model the gas flow in this thesis' work. It provides the transport equations that were solved for the fluid motion, turbulence, energy and species as well as a review of different combustion models.

3.1 Conservation Equations for CFD

Note that vector notation is used for all transport equations. Any vector quantity is expressed in a bold font, such as the velocity vector $\mathbf{u}$. Furthermore, a line over a quantity denotes that it is Reynolds averaged. A Favré averaged quantity is denoted with a tilde.

3.1.1 Conservation of Mass

Conservation of mass for compressible flow is expressed by the continuity equation:

$$\frac{\partial \overline{\rho}}{\partial t} + \nabla \cdot (\overline{\rho}\tilde{\mathbf{u}}) = \dot{S}_M \tag{3.1}$$

where $\dot{S}_M$ is a source term that accounts for evaporation from the liquid phase.

3.1.2 Conservation of Momentum

Conservation of momentum for a compressible fluid is expressed as

$$\frac{\partial \overline{\rho}\tilde{\mathbf{u}}}{\partial t} + \nabla \cdot (\overline{\rho}\tilde{\mathbf{u}}\tilde{\mathbf{u}}) = -\nabla \overline{p} + \nabla \cdot [(\mu + \mu_t)(\nabla \tilde{\mathbf{u}} + (\nabla \tilde{\mathbf{u}})^T] - \nabla \cdot [\frac{2}{3}(\mu + \mu_t)\nabla \tilde{\mathbf{u}}] + \overline{\rho}\mathbf{g} + \dot{\mathbf{S}}_\mathbf{I} \tag{3.2}$$

where $\dot{\mathbf{S}}_\mathbf{I}$ is a source term that accounts for momentum transfer from the liquid phase. Equations 3.1 and 3.2 are often together called the Navier-Stokes equations.

3.1.3 Conservation of Energy

The conservation of energy is expressed as

$$\frac{\partial \overline{\rho}\tilde{h}}{\partial t} + \nabla \cdot (\overline{\rho}\tilde{\mathbf{u}}\tilde{h}) = \frac{D\overline{p}}{Dt} + \nabla \cdot ((\alpha + \alpha_t)\nabla\tilde{h}) + \dot{S}_E + \dot{Q} \tag{3.3}$$

where the contribution of viscous heating and changes in kinetic and potential energy are neglected. The source term $\dot{S}_E$ accounts for energy from the liquid phase. $\dot{Q}$ is a source term that accounts for energy due to a chemical reaction. Note that Equation 3.3 is expressed in sensible enthalpy. An alternative is to express Equation 3.3 as total enthalpy, which would remove the source term $\dot{Q}$ because total enthalpy is conserved over a chemical reaction. Furthermore, α is the thermal diffusivity, which is calculated from on the Prandtl number:

$$\mathrm{Pr} = \frac{\mu}{\rho\alpha} \tag{3.4}$$

3.1.4 Conservation of Species

The conservation of species is expressed as:

$$\frac{\partial \overline{\rho}\tilde{Y_i}}{\partial t} + \nabla \cdot (\overline{\rho}\tilde{\mathbf{u}}\tilde{Y_i}) = \nabla \cdot \left(\left(\overline{\rho} D_i + \frac{\mu_t}{\mathrm{Sc}_t} \right) \nabla \tilde{Y_i} \right) + \dot{\Omega}_i + \dot{S}_{i,E} \tag{3.5}$$

where $\dot{\Omega}_i$ is a source term that accounts for the creation or destruction of a species due to a chemical reaction and $\dot{S}_{i,E}$ is a source term that accounts for evaporation of a fuel from the liquid phase. D_i is the diffusivity and Sc_t is the turbulent Schmidt number. The subscript i denotes different species included in the reaction.

3.2 Turbulence Modeling

At high Reynolds numbers, fluid flows become chaotic and the fluid velocity at one point in space fluctuates around a mean value, seemingly at random. This phenomenon is known as turbulence. The Reynolds number is defined as

$$\mathrm{Re} = \frac{\rho L u}{\mu} \tag{3.6}$$

where L is a characteristic length for the system in question. It can be viewed as the ratio of inertial to viscous forces inside a flowing fluid. Typically, most industrially relevant systems are turbulent, including combustion engines. The Navier-Stokes equations can fully describe a turbulent system, but in practice, this would require that all scales of motion are resolved on a computational mesh. This is known as a direct numerical simulation (DNS). However, resolving the smallest scales of motion is not feasible for most practical applications as this would generate extremely long and memory intensive computations. An alternative to DNS is to express the governing equations of a fluid system in terms of ensemble averaged quantities instead of the

instantaneous ones, then model the impact of turbulence on the mean quantities. This process is commonly known as Reynolds averaging, where the instantaneous velocity is decomposed into its mean value and a fluctuation:

$$\mathbf{u} = \overline{\mathbf{u}} + \mathbf{u}' \tag{3.7}$$

Decomposing the instantaneous velocity according to Equation 3.7, substituting and then performing an ensemble average yields the Reynolds averaged Navier-Stokes (RANS) equations. In this case, the momentum equation has an additional term, R_{ij}, that is not closed:

$$R_{ij} = -\rho\overline{u_i' u_j'} \tag{3.8}$$

This term is known as the Reynolds stress and has to be modeled. The RANS approach is typically used for incompressible flows. However, for a compressible system, it produces more unclosed terms. Therefore, a Favré decomposition is used instead for compressible flows:

$$\mathbf{u} = \tilde{\mathbf{u}} + \mathbf{u}'' \tag{3.9}$$

$$\tilde{\mathbf{u}} = \frac{\overline{\rho\mathbf{u}}}{\overline{\rho}} \tag{3.10}$$

Performing an ensemble average of the Navier-Stokes equation with a Favré decomposed velocity yields one unclosed term:

$$R_{ij} = -\overline{\rho}\widetilde{u_i'' u_j''} \tag{3.11}$$

The stresses in Equation 3.11 can be modeled by the Boussinesq hypothesis, which states that the Reynolds stresses are proportional to the mean rates of deformation [62]:

$$-\overline{\rho}\widetilde{u_i'' u_j''} = \mu_t[\nabla\tilde{\mathbf{u}} + (\nabla\tilde{\mathbf{u}}^T) - \frac{2}{3}\nabla\tilde{\mathbf{u}}] - \frac{2}{3}\overline{\rho}k \tag{3.12}$$

Substituting Equation 3.12 into the Favré averaged Navier-Stokes equations results in Equation 3.2. The turbulent viscosity μ_t is commonly modeled by using the $k-\varepsilon$ model by Launder and Spalding [31], with the eddy viscosity calculated as

$$\mu_t = C_\mu \overline{\rho}\frac{k^2}{\varepsilon} \tag{3.13}$$

The quantities k and ε denote the turbulent kinetic energy and dissipation of turbulence, respectively. To fully close the system, transport equations for these quantities has to be formulated. For this work, an extended formulation of the $k-\varepsilon$ model for compressible flows by Tahry [58] was used.

3.3 Combustion Modeling

This section deals with closing the chemical source terms $\dot{Q}$ and $\dot{\Omega}_i$ in Equations 3.3 and 3.5. In the WSR approach, the chemical source terms are computed directly

from mean quantities, thus ignoring the impact of turbulence-chemistry interactions. Since the timescale for chemical reactions is several orders of magnitude shorter than the timescale for fluid flow, it would be unfeasible to solve the whole CFD system with such a short time step. In the WSR approach, each individual computational cell is treated as a closed homogeneous reactor. The evolution of chemical species in each cell can then be integrated within the current time step using an ODE solver. During the integration, the flow field is considered frozen in time. The updated species composition can then be used to create a linearized source term for each species:

$$\dot{\Omega}_i = \frac{\rho(Y_{i,1} - Y_{i,0})}{\Delta t} \tag{3.14}$$

where $Y_{i,0}$ and $Y_{i,1}$ are the mass fractions of species i before and after integration, respectively. The energy source is given by

$$\dot{Q} = \sum_{i=1}^{n_{\text{Species}}} \frac{h_{298,i}\rho(Y_{i,1} - Y_{i,0})}{\Delta t} \tag{3.15}$$

where h_{298} is the chemical enthalpy at 298 K. The advantage of using the WSR approach is that it is very flexible with respect to the combustion system and does not impose any limitations on the amounts of fuels and sprays that are introduced to the domain. It incorporates the effects of finite rate chemistry and is easy to implement. One of the major downsides of the WSR approach is the computational time: one ODE has to be solved for each chemical species for each computational cell. This can quickly generate unfeasible computational times, and some form of speed up process is necessary to make the solution efficient.

3.3.1 The Combustion Progress Variable Model (CPV)

model was developed and implemented into an external commercial library by LOGE [34] and coupled to OpenFOAM as part of this work. It has previously been successfully applied together with CONVERGE [38] and a 0-D stochastic reactor model [37]. The CPV model assumes that the combustion progress can be parameterized by the pressure, unburned temperature, equivalence ratio and EGR rate. With an appropriately chosen progress variable, the thermochemical state can be reconstructed. The chemical enthalpy h_{298} is used to define a progress variable C:

$$C(t) = \frac{h_{298} - h_{298,u}}{h_{298,min} - h_{298,u}} \tag{3.16}$$

where $h_{298,u}$ is the chemical enthalpy of the unburned mixture and $h_{298,min}$ is the chemical enthalpy of the fully reacted mixture.

A value of $C(t) = 0$ indicates an unburned mixture, whereas $C(t) = 1$ indicates a fully burnt mixture. Using the parameters mentioned above together with the progress variable, a table containing source terms for the progress variable, chemical species, soot and NO_x emissions can be computed using an adiabatic, constant pressure, homogeneous reactor model for a given range of parameters and an appropriate

chemical mechanism. For dual-fuel combustion, two additional parameters are included as dimensions in the table: the fraction of the first fuel and the fraction of the first fuel used in the EGR definition. After the table has been constructed, the source terms can be easily looked up based on the table parameters. This eliminates the need to solve the chemistry during the CFD simulation and also eliminates the need to solve transport equations for every species in the mechanism. Using this approach, it is only necessary to track 14 species that are considered representative for the thermodynamic state of the gas: O_2, N_2, CO_2, H_2O, CO, H_2, C_2H_2, C_2H_4, H, O, OH, N and NO. The progress variable C is not transported directly but is instead calculated based on the mixture fraction Z and h_{298} [38]. Therefore, two additional transport equations are solved by the CFD to compute C:

$$\frac{\partial \overline{\rho}\tilde{Z}}{\partial t} + \nabla \cdot (\overline{\rho}\tilde{\mathbf{u}}\tilde{Z}) = \nabla(\overline{\rho}D\nabla\tilde{Z}) + \overline{\rho\dot{S}_M} \tag{3.17}$$

$$\frac{\partial \overline{\rho}\tilde{h}_{298}}{\partial t} + \nabla \cdot (\overline{\rho}\tilde{\mathbf{u}}\tilde{h}_{298}) = \nabla \cdot (\overline{\rho}D\nabla\tilde{h}_{298}) + \overline{\rho\dot{S}_{M,h_{298}}} + \overline{\rho\dot{S}_{Chem,h_{h298}}} \tag{3.18}$$

where $\overline{\dot{S}_M}$ and $\overline{\dot{S}_{M,h_{298}}}$ are source terms arising due to fuel injection, and $\dot{S}_{Chem,h_{h298}}$ is a source term due to chemical reaction, taken from the CPV table.

Chapter 4

Spray Modeling Approach

This chapter introduces the methodology used to model the liquid spray formation in this thesis' work.

4.1 Eulerian-Lagrangian Approach

The Eulerian-Lagrangian approach refers to a type of multi-phase modeling where the continuous phase is described in a Eulerian frame of reference and the dispersed phase is described in a Lagrangian frame of reference. A Eulerian frame of reference uses a control volume that is fixed in space. The properties of the control volume can change with time. In a Lagrangian frame of reference, the control volume changes in time and moves with the flow field. A Eulerian frame of reference is suitable for media that can be described as a continuum, whereas a Lagrangian frame of reference is the natural way to describe discrete particles. Sprays are commonly modeled using the Eulerian-Lagrangian approach.

4.2 Stochastic Blob & Bubble Model

In this work, the stochastic blob & bubble model (VSB2) was used to model the spray development and formation. This model has previously been used to successfully model the formation of diesel sprays in both OpenFOAM and STAR-CD[17, 28, 29]. The main difference between this model and other Eulerian-Lagrangian spray models is that instead of each Lagrangian parcel representing a collection of identical droplets, the model defines the concept of an irregular blob representing a collection of different droplet sizes. This difference is illustrated schematically in Figure 4.1. The model has been designed to use a minimum number of tuning parameters and can be implemented in any CFD code that features particle tracking.

4.2.1 VSB2 Primary Breakup: Blob injection

The impact of primary breakup on the spray in VSB2 is modeled in a simple way using the concept of blob injection. In blob injection, no model is used for primary

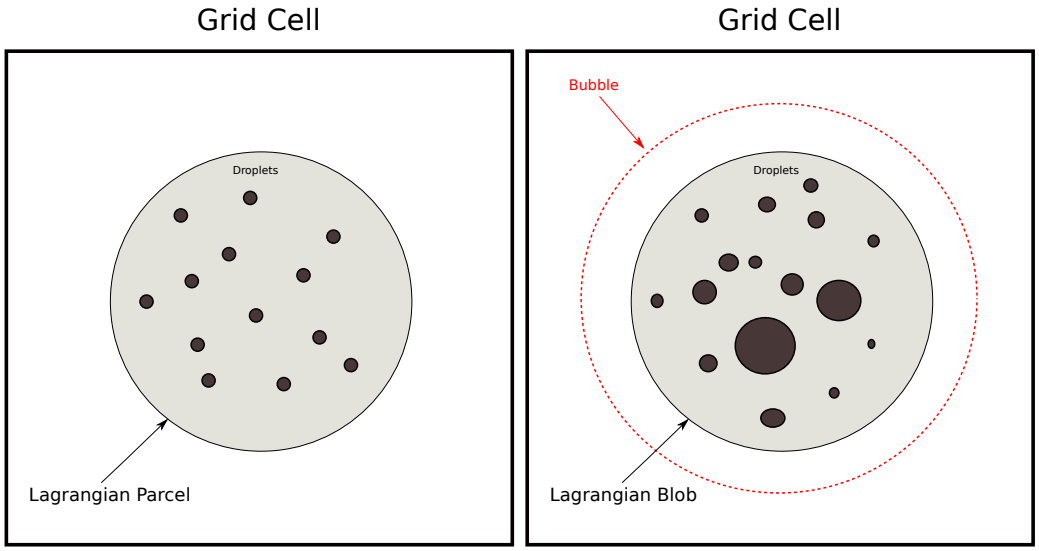

(a) Traditional Spray Model (b) VSB2

Figure 4.1: Illustration of the difference between VSB2 and traditional Eulerian-Lagrangian spray models

breakup. Instead, the computational blobs are injected into the domain with the same diameter as the injector nozzle.

4.2.2 VSB2 Secondary Breakup: Distribution Function

The impact of secondary breakup on the spray in VSB2 is modeled by a distribution function. The distribution of droplet sizes inside each Lagrangian blob is governed by a one-parameter, power-law cumulative distribution function:

$$D_{\text{Norm}} = M_{\text{Norm}}^{f}, \qquad M_{\text{Norm}} \in [0,1], \qquad f > 0 \tag{4.1}$$

where D_{Norm} is the droplet diameter normalized by the largest droplet size, D_{Blob}. The maximum droplet size can be calculated each time step by first allowing the unstable droplets to change according to the rate equation by Reitz and Diwakar [51]:

$$\frac{dD_{\text{Blob}}}{dt} = -\frac{D_{\text{Blob}} - D_s}{\tau_{\text{Breakup}}} \tag{4.2}$$

By integrating Equation 4.2 over a computational time step, the updated blob size, D'_{Blob} can be calculated. This represents the new maximum droplet size one time step later. D_s is the stable droplet diameter at the local conditions and τ_{Breakup} is the breakup time, which is obtained from the breakup rate correlations by Pilch and Erdman [44]. The stable droplet diameter can be calculated based on the critical Weber number:

$$D_s = \frac{\text{We}_{\text{Cr}}\sigma}{\rho_g U_{\text{Rel}}^2} \tag{4.3}$$

The critical Weber number can be obtained from the following correlation with the Ohnesorge number by Pilch and Erdman [44]:

$$\mathrm{We_{Cr}} = 12(1 + 1.077\mathrm{Oh}^{1.6}) \tag{4.4}$$

The Ohnsorge number relates viscous forces to inertial and surface tension forces, and is defined as:

$$\mathrm{Oh} = \frac{\sqrt{\mathrm{We}}}{\mathrm{Re}} \tag{4.5}$$

The power law coefficient f in Equation 4.1 can be calculated from the values of D_s and m_s, which are first normalized by the maximum droplet size and the mass of the entire blob:

$$D_{s,\mathrm{Norm}} = \frac{D_s}{D_{\mathrm{Blob}}} \tag{4.6}$$

$$M_{s,\mathrm{Norm}} = \frac{m_s}{m_{\mathrm{Blob}}} = \frac{D^3_{\mathrm{Blob}} - D'^3_{\mathrm{Blob}}}{D^3_{\mathrm{Blob}}} = 1 - \left(\frac{D'_{\mathrm{Blob}}}{D_{\mathrm{Blob}}}\right)^3 \tag{4.7}$$

Where the stripped off mass m_s is given by:

$$m_s = \rho_l \frac{\pi}{6}\left(D^3_{\mathrm{Blob}} - D'^3_{\mathrm{Blob}}\right) \tag{4.8}$$

The power law coefficient can then be calculated by evaluating Equation 4.1 at $D_{s,\mathrm{Norm}}$ and $M_{s,\mathrm{Norm}}$:

$$f = \frac{\log(D_{s,\mathrm{Norm}})}{\log(M_{s,\mathrm{Norm}})} = \frac{\log\left(\frac{D_s}{D_{\mathrm{Blob}}}\right)}{\log\left[1 - \left(\frac{D'_{\mathrm{Blob}}}{D_{\mathrm{Blob}}}\right)^3\right]} \tag{4.9}$$

With Equation 4.1 being fully defined, we now have a distribution function for each Lagrangian blob. The shape of the function depends on the local breakup conditions and is parameterized by the breakup time and the critical Weber number. Examples of different possible shapes of the CDF are shown in figure 4.2, with three different lines representing strong breakup (generating many small droplets), weak breakup (generating fewer larger droplets) and an intermediate case between the two. Furthermore, in this work, the CDF was split into 10 different droplet mass intervals (figure 4.2). The first interval was defined by the stable droplet diameter and the stripped off mass. The remaining 9 intervals were split equally between the stripped off mass and the maximum droplet mass. A droplet size was sampled randomly in each interval, and the sampled droplet sizes were chosen to interact with the gas phase.

4.2.3 Gas Phase Coupling

Coupling between the liquid and gas phase was achieved through source terms on the transport equations for mass, energy and momentum, as described in Chapter

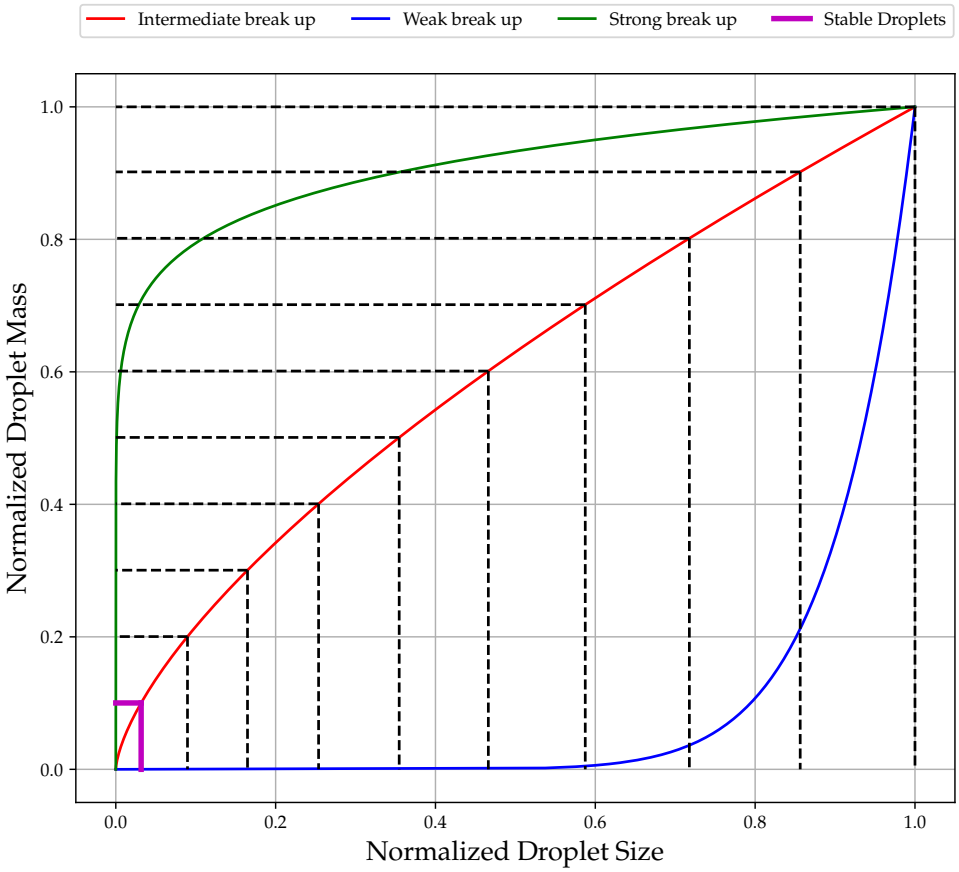

Figure 4.2: Examples of CDF shapes for different break up conditions

3. The transfer of mass and energy from the liquid to the gas phase was achieved through relaxation equations:

$$\frac{dm_{\mathrm{Evap},i,j}}{dt} = \frac{m_{\mathrm{Eq},j} - m_{\mathrm{blob},i,j}}{\tau_{m,i,j}} \tag{4.10}$$

$$\frac{dT_{\mathrm{Blob}}}{dt} = \sum_{i=1}^{n_{\mathrm{Blob}}} \frac{T_{\mathrm{Eq}} - T_{\mathrm{blob}}}{\tau_{T,i}} \tag{4.11}$$

The relaxation equations were solved for each droplet size, and the total contribution was summed to give the final change in mass and energy. Note that the subscript i denotes a different droplet size interval, whereas the subscript j denotes different fuel components in a multi-component fuel blend. In contrast to gradient based mass and heat transfer models, the relaxation equations prevent over- and undershoots in the transfer of mass and energy to the gas phase because the calculated equilibrium mass $m_{\mathrm{Eq},j}$ and temperature T_{Eq} give a theoretical maximum change based on phase-equilibrium thermodynamics. The relevant relaxation times were

obtained from dimensional analysis [24]:

$$\tau_{m,i,j} = \frac{\rho_l D_{\text{Blob},i}^2 R T_f}{6 P D_j \text{Sh}} \tag{4.12}$$

where T_f is the liquid film temperature, D_j is the diffusion coefficient and Sh is the Sherwood number.

$$\tau_{T,i} = \frac{\rho_l, D_{\text{Blob},i}^2 C_{p,\text{blob}}}{6 \lambda f_Z \text{Nu}} \tag{4.13}$$

where λ is the thermal conductivity of the liquid film, f_Z is a correction factor that accounts for the influence of mass transfer on the heat transfer coefficient by El Wakil et al. [12] and Nu is the Nusselt number. The Nusselt and Sheerwood numbers were calculated from the correlations by Ranz and Marshall [49]:

$$\text{Sh} = 2 + 0.6 \text{Re}^{1/2} \text{Sc}^{1/3} \tag{4.14}$$

$$\text{Nu} = 2 + 0.6 \text{Re}^{1/2} \text{Pr}^{1/3} \tag{4.15}$$

The equilibrium mass was calculated using an iterative solution procedure where small amounts of mass were evaporated until the gas reaches saturation. Alternatively the thermodynamic equations can be solved as a coupled system using a non-linear equation solver. This is necessary for cases where the liquid consists of multiple components.

The transfer of momentum to the gas phase was handled in a more traditional way with a force balance over the gas liquid interface:

$$m_{\text{Blob}} \frac{dU_{\text{Blob}}}{dt} = \sum_{i=1}^{n_{\text{Blob}}} \frac{\pi}{8} D_i^2 \rho_g C_D |U_g - U_{\text{Blob}}| (U_g' - U_{\text{Blob}}') \tag{4.16}$$

where the U_g' and U_{Blob}' denote the velocity of the gas and blob, respectively, at the next time step. Note that drag was the only interface force considered as all other interface forces were considered negligible compared to drag. The drag coefficient C_D was given by the following correlation by Schmehl et al. [53]:

$$\begin{aligned} C_D = \quad & 0.28 + \frac{21}{\text{Re}_i} + \frac{6}{\sqrt{\text{Re}_i}} + \text{We}(0.2319 - 0.1579 \log(\text{Re}_i) \\ & + 0.0471 \log^2(\text{Re}_i) \ - 0.0042 \log^3(\text{Re}_i)) \qquad \text{Re}_i < 2000 \qquad (4.17) \\ C_D = \quad & 0.424 \qquad \text{Re}_i \geq 2000 \qquad (4.18) \end{aligned}$$

The contribution of each droplet size was calculated and summed to give the total momentum of the blob.

4.2.4 Child Blobs From Stripped off Droplets

A problem with the approach that was described in the previous section arises when the momentum coupling with the gas phase was calculated. The blobs contain a distribution of different droplet sizes that contribute to the mass, energy and

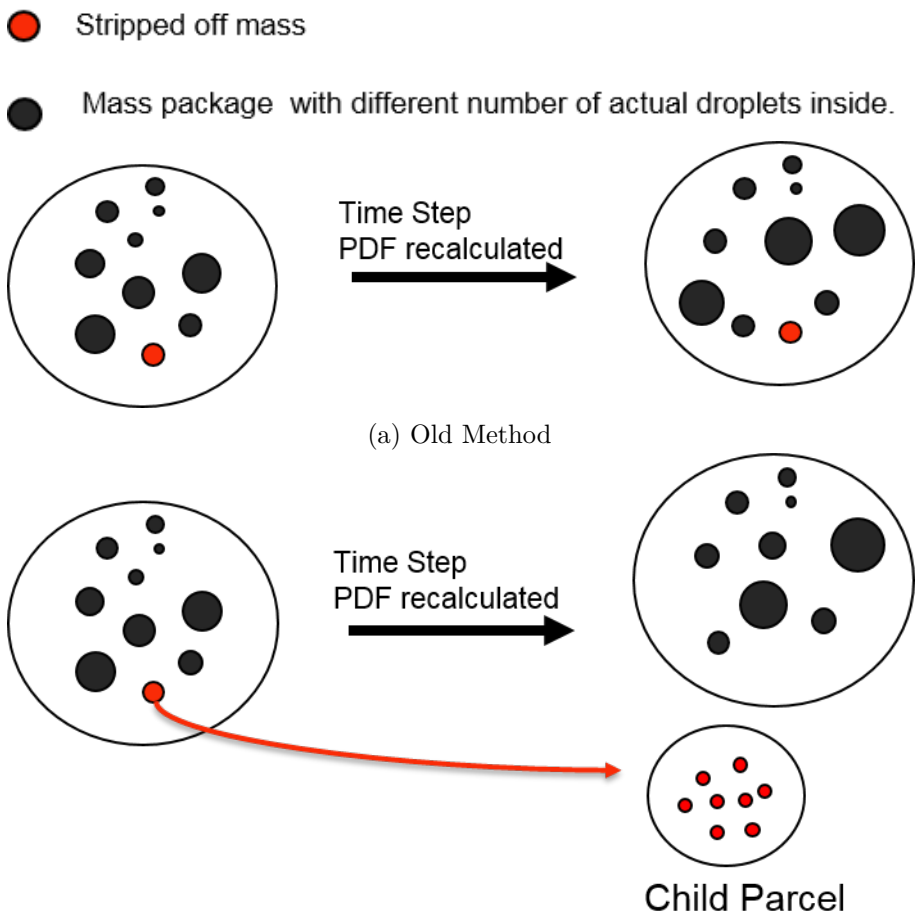

(a) Old Method

(b) New Method

Figure 4.3: Illustration of the improved break up treatment

momentum exchange with the gas phase. However, when the computational blobs are advanced during the simulation all droplet sizes will have the same properties as the computational blob. This is strictly speaking not accurate, and a consequence of this was that smaller stable droplets will have the same momentum as the larger unstable droplets. As part of the work in this thesis, an extension to the breakup treatment was proposed were the stable droplets inside each computational blob are used to create a child blob, containing only stable droplets. The procedure is illustrated in 4.3. The methodology was evaluated in papers 2 and 3.

4.3 Bubble Definition

As shown in Figure 4.1, the model featured the concept of a bubble. The bubble imposes a limit on the amount of gas mass that the liquid phase could interact with. This can reduce the grid dependency on coarser grids. The volume of the bubble was defined as:

$$V_{\text{Bubble}} = N_D \rho_g \frac{\pi}{4} D_B^2 l_{\text{diff}} \tag{4.19}$$

where N_D is the initial number of droplets in the blob, D_B is the gross droplet size based on the mass of the blob. The size of the bubble was further governed based on the local turbulent diffusion length scale:

$$l_{\text{diff}} = \sqrt{\frac{\mu_t}{\rho_g} dt_s} \tag{4.20}$$

Where dt_S is the sub-cycle time step. It should be noted that the maximum possible bubble size was limited to the grid size. Thus, for most of the work presented in this thesis, the computational cells were used instead of the bubble due to the fine cell sizes used.

Chapter 5

Summary of Results

This chapter summarizes the results presented in the papers appended to this thesis. The focus is on Papers 1, 2 and 5, where the author of this thesis was the main contributor. However, Papers 3 and 4 will also be briefly summarized. All simulations were made using OpenFOAM-2.2.x [63].

5.1 Paper 1:

This paper explored and validated the performance of the VSB2 spray model together with ethanol. Several different mesh sizes and turbulence parameters were considered to evaluate the performance of the model and tune the turbulence parameters.

5.1.1 Case Summary

Data from the Chalmers high-pressure, high-temperature spray chamber were used to validate the VSB2 spray model for use with alcohol sprays and to tune the turbulence parameters. Two experimental conditions were considered, which are summarized in Table 5.1. The spray chamber was represented as a cylinder, and simulations were conducted on two different grids, shown in Figure 5.1. The coarse grid consisted of 224 750 cells, whereas the fine grid consisted of 1 190 100 cells.

Table 5.1: Ambient conditions for Chalmers HP/HT spray chamber

	Case 1	Case 2
Ambient Temperature (^{o} C)	550	425
Ambient Pressure (bar)	60	54
Gas Density (kg/m^3)	25.4	27
Injection Pressure (bar)	1000	1000
Injection Duration (μs)	1500	1500

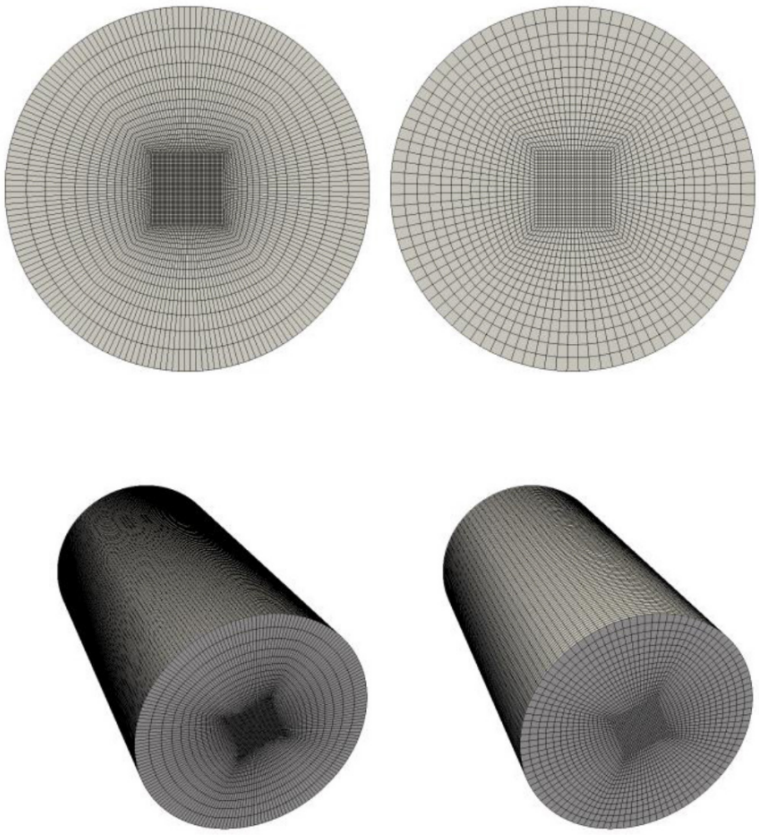

Figure 5.1: The two grids (fine and coarse) used to study the ethanol spray.

5.1.2 Mesh Dependency

The coarse grid had an edge size of 0.5 mm in the center, whereas the fine mesh had an edge size of 0.25 mm. The effects of the grid size on the liquid and vapor penetration lengths are shown in Figure 5.2. It was found that there was virtually no difference in the stable liquid penetration length between the two meshes, but there was a small difference in the initial transient phase. This can be explained by a greater effect of numerical diffusion on the vapor field upstream close to the injector, where the size of the vapor field is much smaller in the radial direction.

5.1.3 Tuning the Turbulence Parameters

The model was first tested with the standard values for the $k-\varepsilon$ model, which are presented in Table 5.2. The results for case A are shown in Figure 5.3. It can be seen that the liquid penetration was predicted well by the standard coefficients, but the vapor penetration was under-predicted. The inability to predict the formation of a round jet is a well-known limitation of the $k-\varepsilon$ model. An attempt was made to tune the spray model by increasing C_1 to 1.55 and letting σ_ε vary with C_1 according to R. [47]. The tuned $k-\varepsilon$ coefficients are shown in Table 5.3. The results are shown in Fgure 5.4, which show that tuning the coefficients resulted in better agreement for

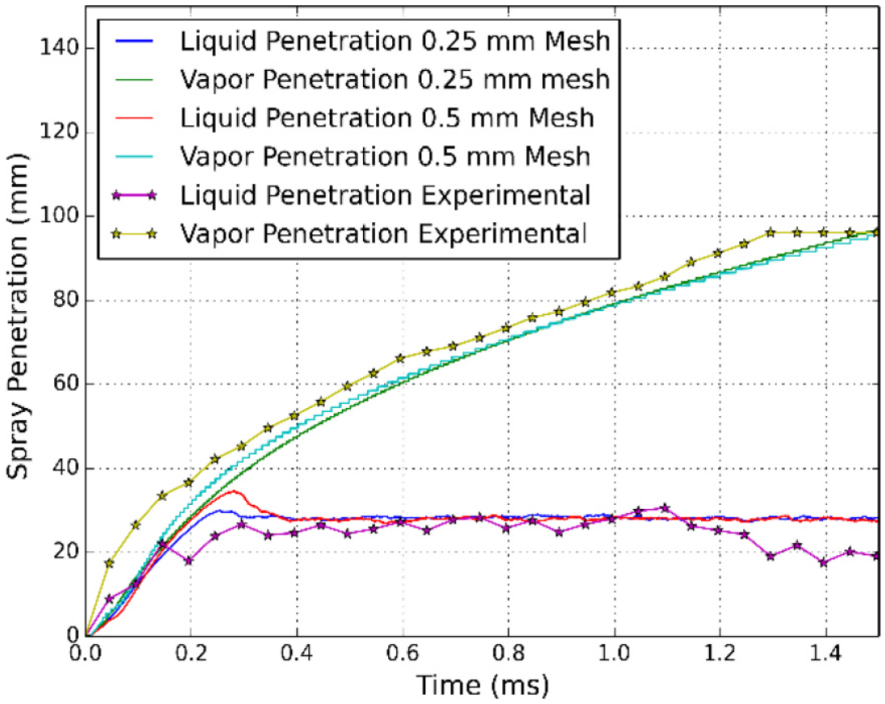

Figure 5.2: Comparison of spray penetration for a fine and coarse mesh.

the vapor penetration. Values of 1.55-1.6 for C_1 are consistent with other studies in the literature [59, 14].

Table 5.2: Standard Coefficients of the $k-\varepsilon$ model.

C_1	C_2	C_3	C_μ	σ_ε	σ_k
1.44	1.92	-0.33	0.09	1.257	1

Table 5.3: Tuned Coefficients of the $k-\varepsilon$ model.

C_1	C_2	C_3	C_μ	σ_ε	σ_k
1.55	1.92	-0.33	0.09	1.529	1

5.1.4 Influence of fixing the length scale in the injector cell

The influence of fixing the turbulent length scale in the injector cell was also investigated. The turbulent length scale was fixed to 10 % of the injector nozzle diameter. This was done to impose a boundary condition on turbulence in the injection cell. The length scale was fixed by selecting the value of ε in the injection cell. The results of this is shown in figure 5.5. The results are presented in Figure 6.4, which shows that without fixing the turbulent length scale, the liquid penetration was over-predicted. A similar observation was made by Kösters and Karlsson [28] for diesel sprays.

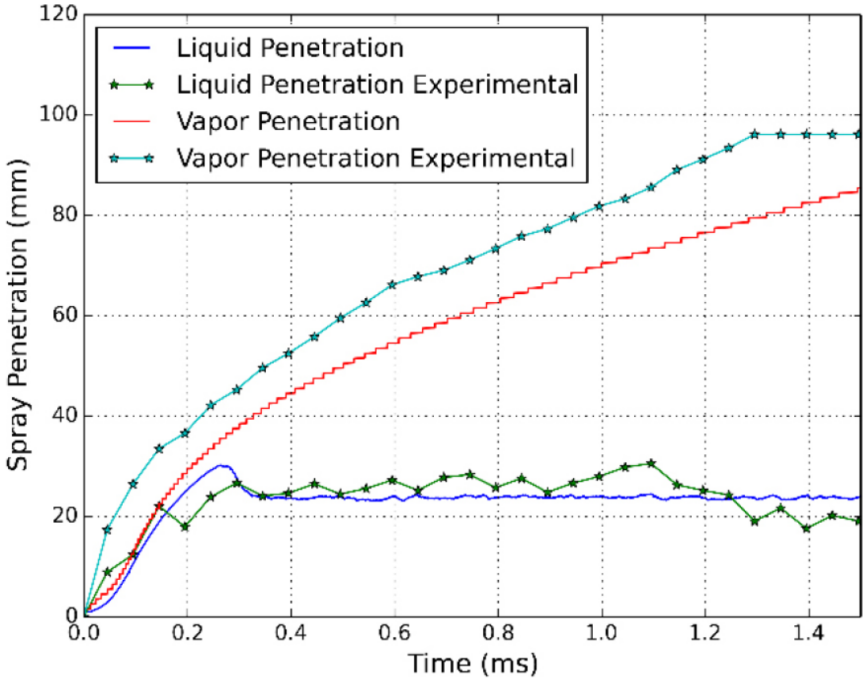

Figure 5.3: Spray penetration of the ethanol spray using the VSB2 spray model with standard coefficients in the turbulence model.

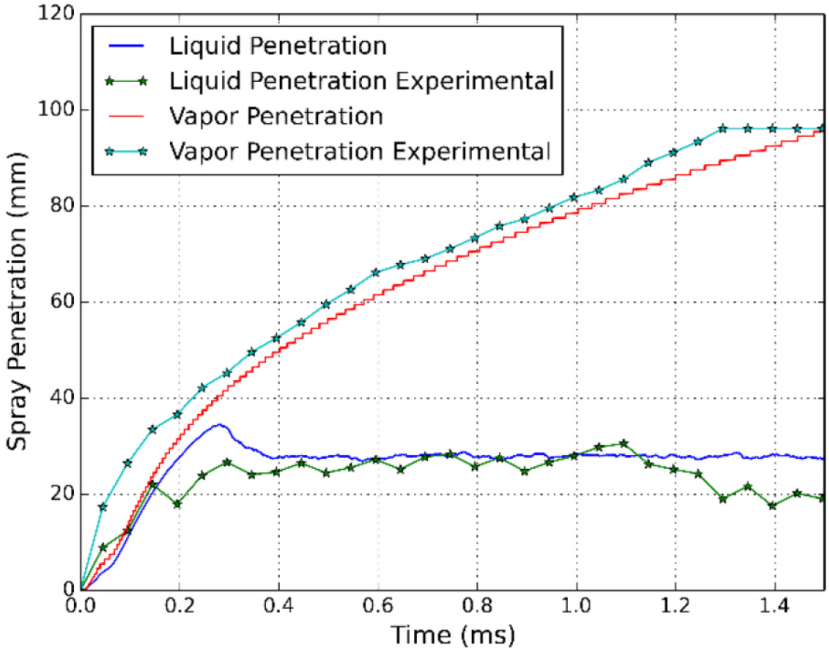

Figure 5.4: Spray penetration of the ethanol spray using the VSB2 spray model with tuned coefficients in the turbulence model.

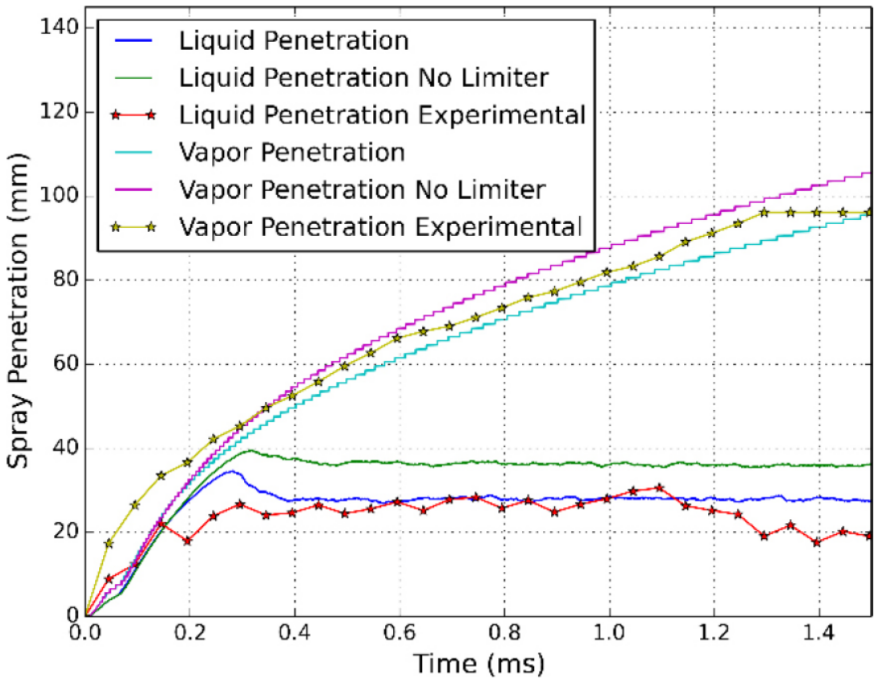

Figure 5.5: Spray penetration of the ethanol spray using the VSB2 spray model with or without fixing the turbulent length scale in the injector cell.

5.1.5 Paper 1 Conclusions

For the study in paper 1, it was concluded that the VSB2 model can accurately model the spray penetration of ethanol. Furthermore, tuning the constants of the $k-\varepsilon$ model gave better agreement with the experimental data. It was also concluded that it is necessary to fix the turbulent length scale in the injector cell for accurate prediction of the liquid penetration. In addition to the results presented here, we also examined the influence of initial turbulence and changing from the standard $k-\varepsilon$ model to the realizable $k-\varepsilon$ by Shih et al. [56]. It was concluded that varying the initial turbulence by an order of magnitude did not change the prediction of spray penetration in any significant way. Switching to the realizable model resulted in worse agreement with experimental data but slightly better prediction of the initial transience in liquid penetration.

5.2 Paper 2

In chapter 4, a shortcoming of how the VSB2 model handles the blob momentum was introduced. A possible remedy to the issue was presented in the form of creating child blobs based off the stable droplets in the blob at the local conditions. In the study presented in paper 2, the proposed method was investigated by comparing the old breakup treatment with the new one at two different experimental conditions. The hypothesis was that by more accurately representing the momentum of the stable droplets, the evaporation and dispersion characteristics of the spray would be

Table 5.4: Ambient conditions for the ECN Spray A cases

	Case A	Case B
Ambient Temperature (K)	900	700
Ambient Pressure (bar)	60.5	46
Gas Density kg/m^3	22.9	22.9

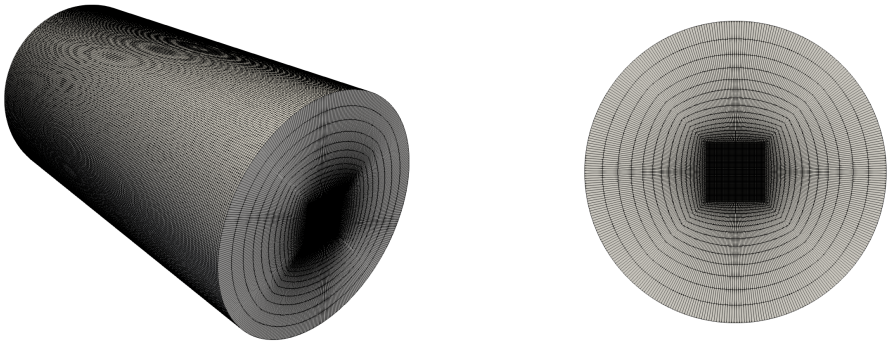

Figure 5.6: Computational mesh used in the ECN Spray A cases

better predicted by the model. The main objective of this study was to asses the impact of the new breakup treatment on spray parameters such as liquid- and vapor penetration, evaporation rate and vapor dispersion.

5.2.1 Case Summary

Data from the Engine Combustion Network (ECN)[13] were used to validate the improved breakup treatment developed for the VSB2 spray model. The ECN Spray A refers to a n-dodecane spray that is injected into a spray chamber under diesel-engine-like conditions. Two reference cases from the ECN database was chosen. The two cases simulated are summarized in 5.4. The simulations were performed on a very fine grid consisting of 3 294 060 cells 5.6.

5.2.2 Liquid Penetration

Figures 5.7 and 5.8show the liquid penetration for case A and B, respectively. The new breakup treatment improved the prediction of the liquid penetration slightly in case A and with a much more pronounced effect in case B. The reason for this was likely the lower ambient temperature in case B. The new breakup treatment generated a larger number of small Lagrangian blobs containing small stable droplets. The small size of these droplets facilitates their evaporation. It is likely that due to the higher ambient temperature in case A, the droplets evaporate anyway.

5.2.3 Vapor Penetration

Figures 5.9 and 5.10 show the vapor penetration for case A and B. It was found that the new breakup treatment had virtually no effect on the prediction of the vapor

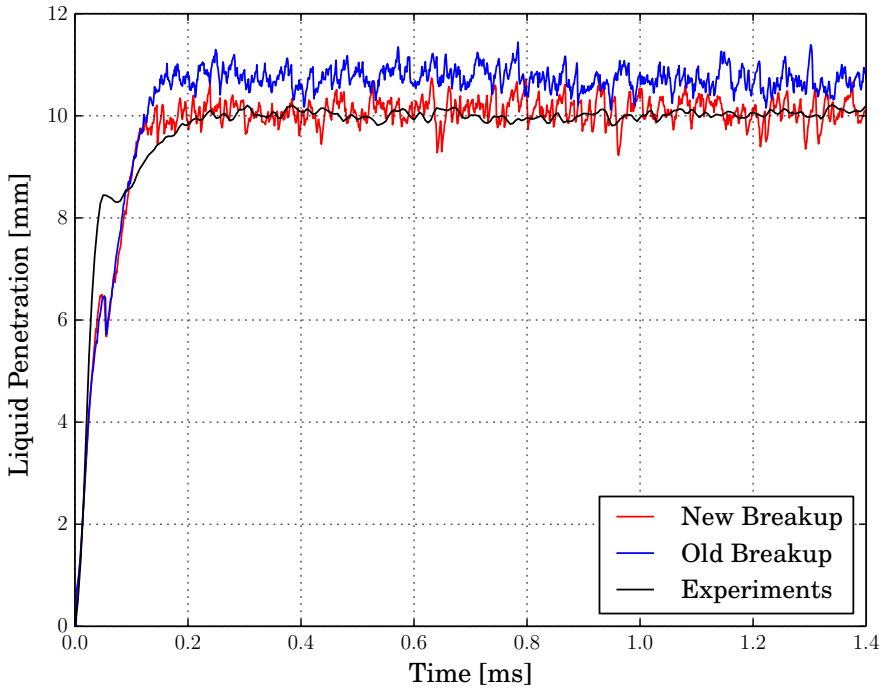

Figure 5.7: Comparison of the liquid penetration between the new and the old breakup treatment for case A

penetration.

5.2.4 Evaporation Rate

Figures 5.11 5.12 show the evaporation rate for both case A and B. It can be seen that the evaporation rates for the old and new breakup treatments were very similar for case A, but for case B, the evaporation rate of the spray was slightly higher for the new breakup treatment. Thus introducing child blobs seem to enhance evaporation in the low temperature case.

5.2.5 Radial Concentration

The effect on the radial concentration of fuel was also investigated. Figures 5.13 and 5.14 shows the radial concentration for case B at 8 mm and 11 mm downstream from the injector. It can be seen that the dispersion of the vapor increased downstream as a result of the new breakup treatment. This effect was likely due to the formation of smaller blobs with stable droplets. The smaller droplets have a lower relative velocity and are more easily dispersed by the bulk flow.

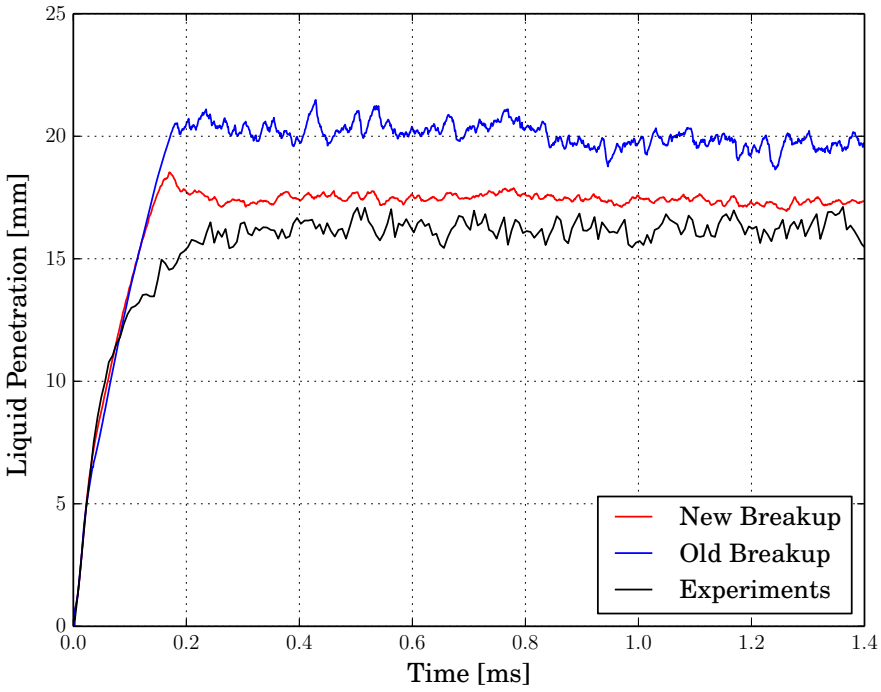

Figure 5.8: Comparison of the liquid penetration between the new and the old breakup treatment for case B

5.2.6 Paper 2 conclusions

In this paper the effect of creating child blobs from the stable droplets on the characteristics of the spray was investigated. This addresses a fundamental flaw in the model that was present previously. The study showed that the new breakup treatment seem to enhance the evaporation and dispersion of the spray in the lower temperature case, but it has a much smaller effect on the high temperature case. Furthermore, the predicted liquid penetration agreed better with the experimental data in the lower temperature case. It can be theorised that in the higher temperature case, that the surrounding gas has enough energy that the enhanced evaporation from the presence of smaller blobs is negligible. In addition to the results presented here, turbulence levels were also studied. It was shown that the predicted maximum turbulence levels were lower with the new breakup treatment. It was concluded that this could be due to smoother velocity gradients created by the dispersed phase due to the smaller blobs from the stripped off mass being more affected by drag forces.

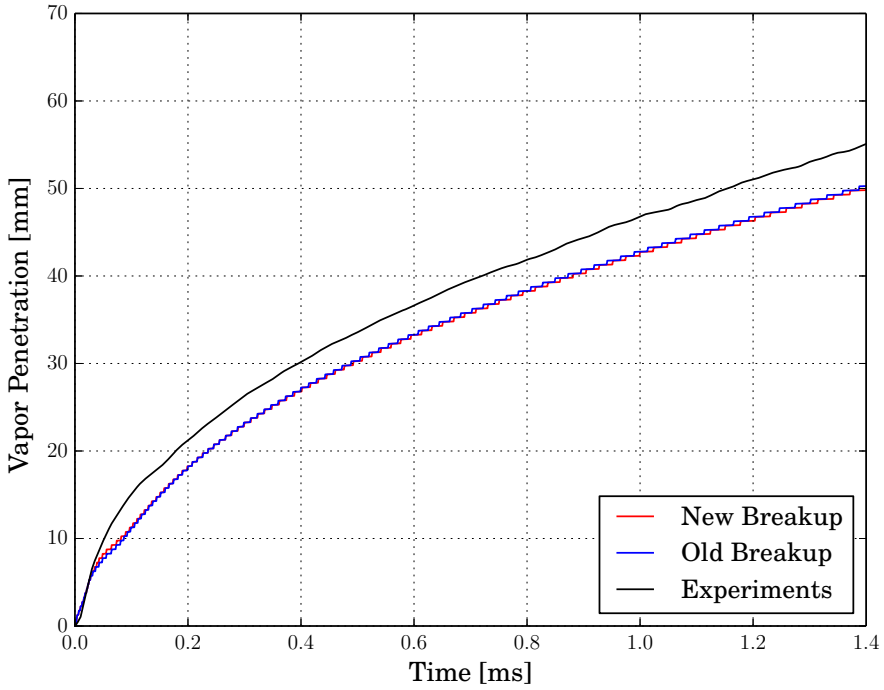

Figure 5.9: Comparison of the vapor penetration between the new and the old break up treatment for Case A

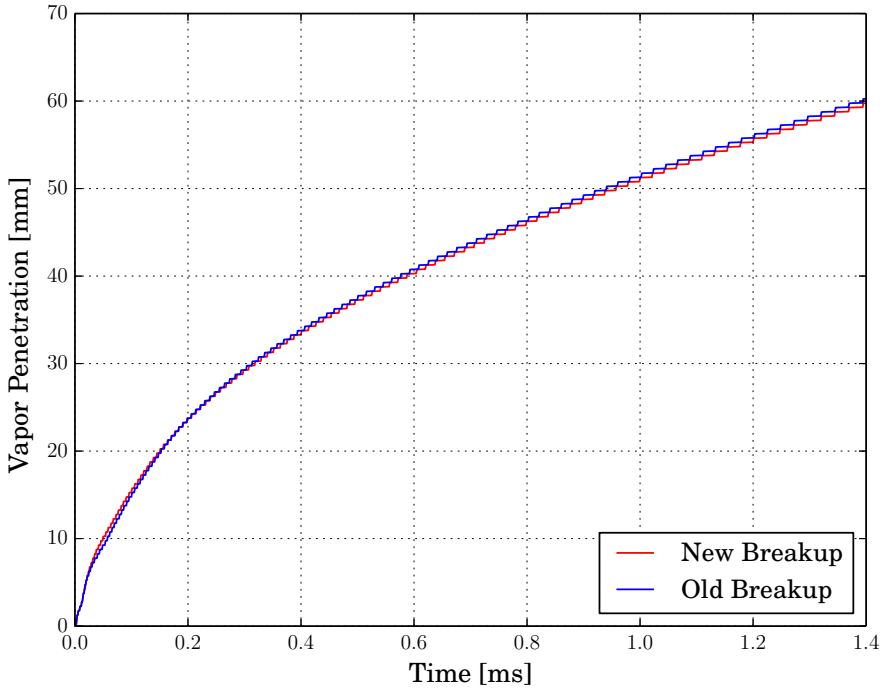

Figure 5.10: Comparison of the vapor penetration between the new and the old break up treatment for Case B

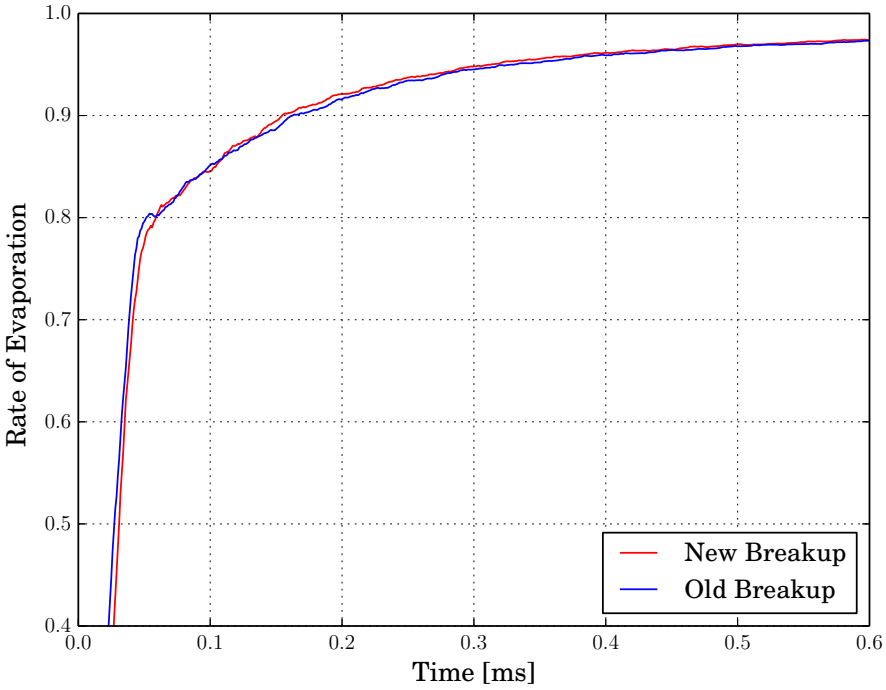

Figure 5.11: Comparison of the evaporation rate between the new and old breakup treatments for case A

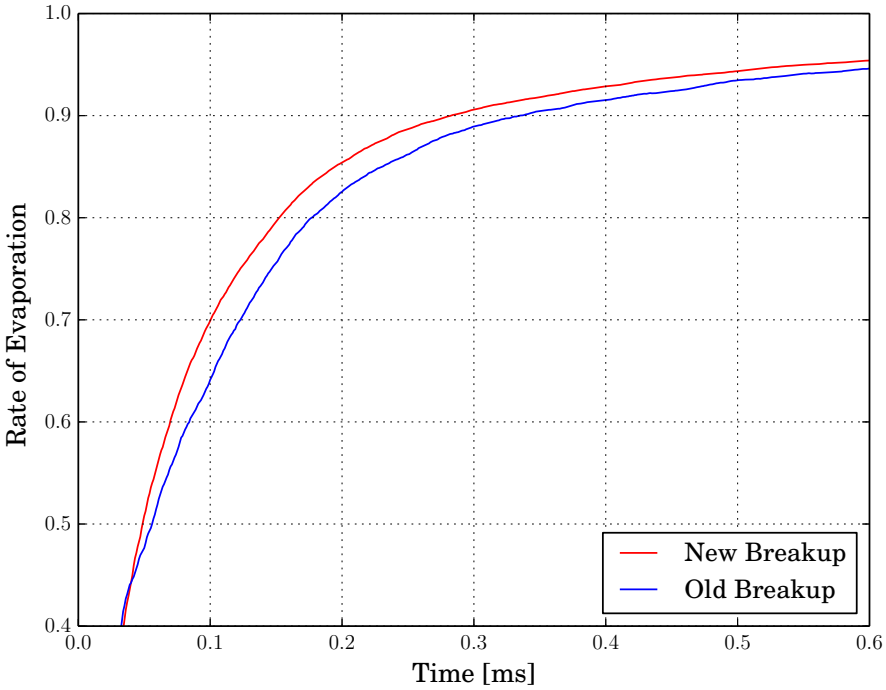

Figure 5.12: Comparison of the evaporation rate between the new and old breakup treatments for case B

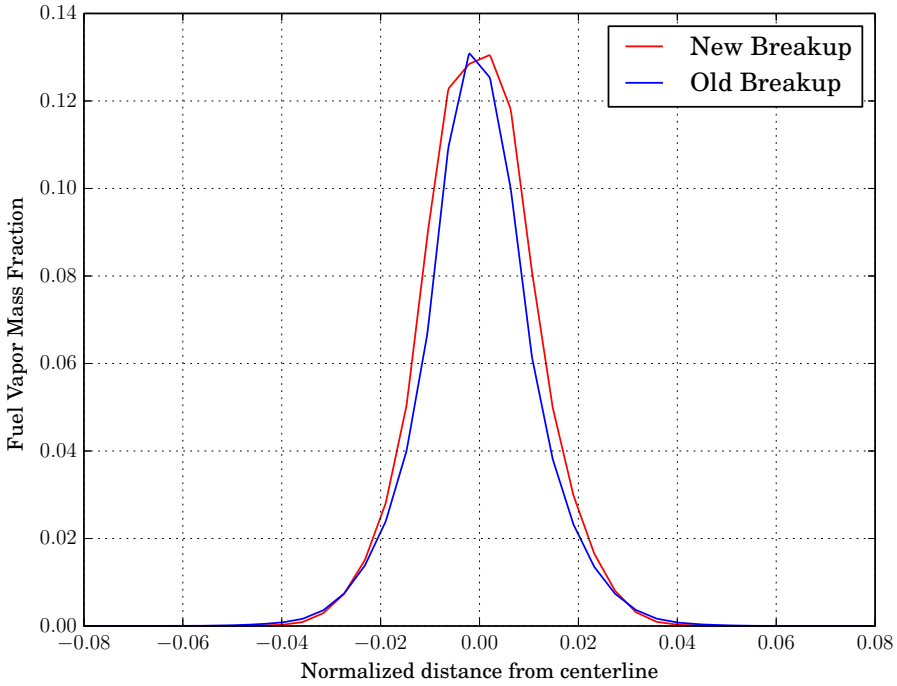

Figure 5.13: Radial concentration profile of n-dodecane in Case B 8mm downstream from the injector.

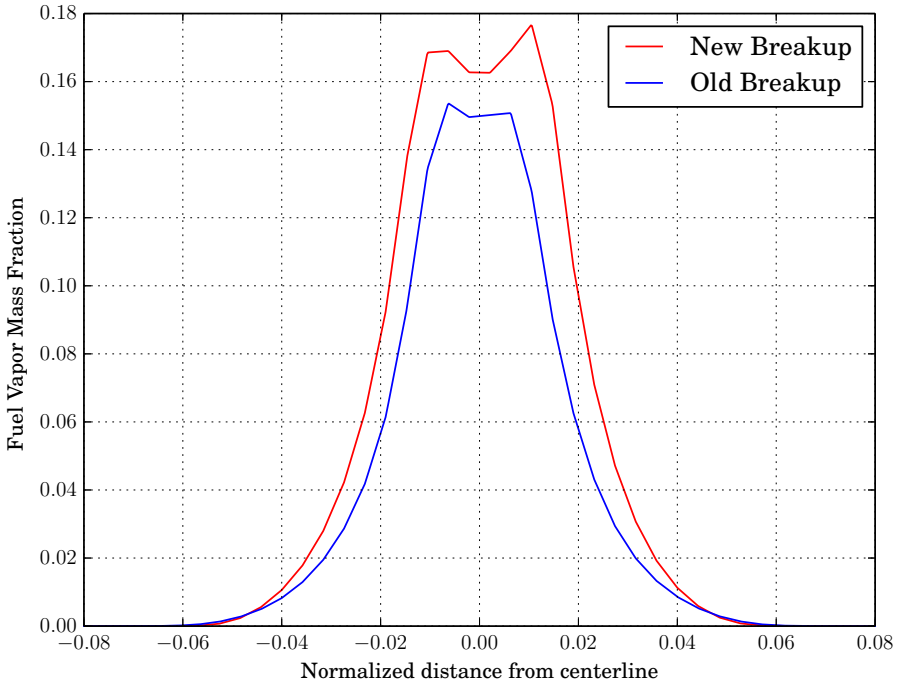

Figure 5.14: Radial concentration profile of n-dodecane in Case B 11mm downstream from the injector.

5.3 Paper 3

Paper 3 presented a comprehensive study of the impact of resolving the injector orifice and influence of created stripped off droplets. The author of this thesis contributed to this work by developing the improved breakup treatment used to create the stripped off droplets, which was a continuation of the development presented in Paper 2. In this paper the effect of the new break up treatment on the droplet size was further investigated by comparing the Sauter mean diameter (SMD) both with and without the new breakup treatment. SMD is defined as:

$$\mathrm{SMD} = \frac{\sum_{i=1}^{N_{\mathrm{par}}} \sum_{j=1}^{n_{\mathrm{blob}}} m_j D_j^3}{\sum_{i=1}^{N_{\mathrm{par}}} \sum_{j=1}^{n_{\mathrm{blob}}} m_j D_j^2} \tag{5.1}$$

where i refers to a computational blob and j refers to a specific size interval in the droplet size distribution. N_{par} is the number of blobs in the system, n_{blob} is the number of droplet size intervals and D_j is the diameter of a given droplet size interval. A comparison of the SMD between the new and old breakup treatments for the same conditions as case A in paper 2 is shown in figure 5.15. It is shown that the SMD is lower with the new break up treatment, showing that blobs have a larger surface area per volume unit, and thus evaporates slightly faster. Figure 5.16 show a glyph representation of the Lagrangian blobs, sized according to the blob mass. It can be seen here that the stripped off case with the new breakup treatment produced a lot more smaller blobs than the non-stripped off case. The study concluded that the new breakup treatment produced a larger amount of Lagrangian blobs with a smaller SMD than the old breakup treatment. I was also concluded that this had very little effect on the spray penetration. However, only a high temperature case at 900 K was considered. The results also confirmed the findings in Paper 2. The impact of resolving the shape of the injector nozzle into 9 different computational cells was also studied. It was concluded that the resolved nozzle mesh predicted a liquid penetration close to experimental values. Also, the resolved nozzle mesh predicted finer structures in the spray that were not seen in the unresolved case.

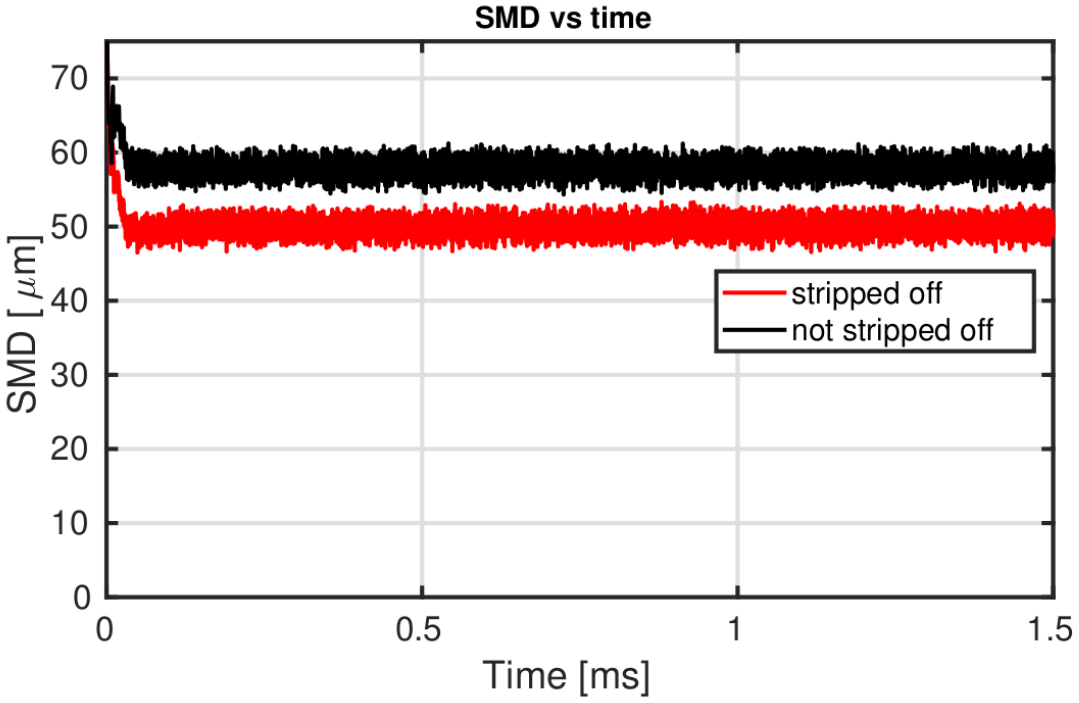

Figure 5.15: Comparison of SMD between the old and new breakup treatment.

(a) Unstripped off case

(b) Stripped off case

Figure 5.16: Glyph representation of spray at 0.1ms ASOI sized ac- cording to blob mass

5.4 Paper 4

Paper 4 presented a comprehensive experimental study of a direct-injection dual-fuel engine operated with methanol and ethanol as a main fuel. The author of this thesis contributed to this work by performing CFD simulations to identify where flame-wall and flame-flame interactions occurred. They also performed injection rate meter tests that were used to analyze the rate of heat release.

The experiments conducted in this study showed that the alcohol fuels significantly outperformed diesel in all cases. The indicated thermal efficiency was increased by up to 3.5 % and NO_x emissions were reduced by up to 20 %. Furthermore, soot emissions were decreased by a factor of 40 and were virtually non-existent in the methanol tests.

A comprehensive analysis of the rate of heat release was presented for a mid-load case at 1262 RPM and 172 Nm. Figure 5.17 shows the stoichiometric surface of methanol colored by temperature. It indicates that the flame-wall interactions started at approximately 2.9 CAD aTDC, and the flame-flame interactions started at approximately 5.0 CAD aTDC. This matched the changes in the slope of the aRoHR, indicating that such interactions occurred. Figure 5.17 also shows the measured apparent rate of heat release compared to the measured injection rate of the main fuel. It was found that the rise in rate of heat release corresponded to the rise in injection rate, indicating that the ignition delay was very short. The bottom plot in Figure 5.17 shows the trigger signals recorded by both the engine and injection rate meter, indicating that the measured injection rate was comparable to the injection rate in the actual engine.

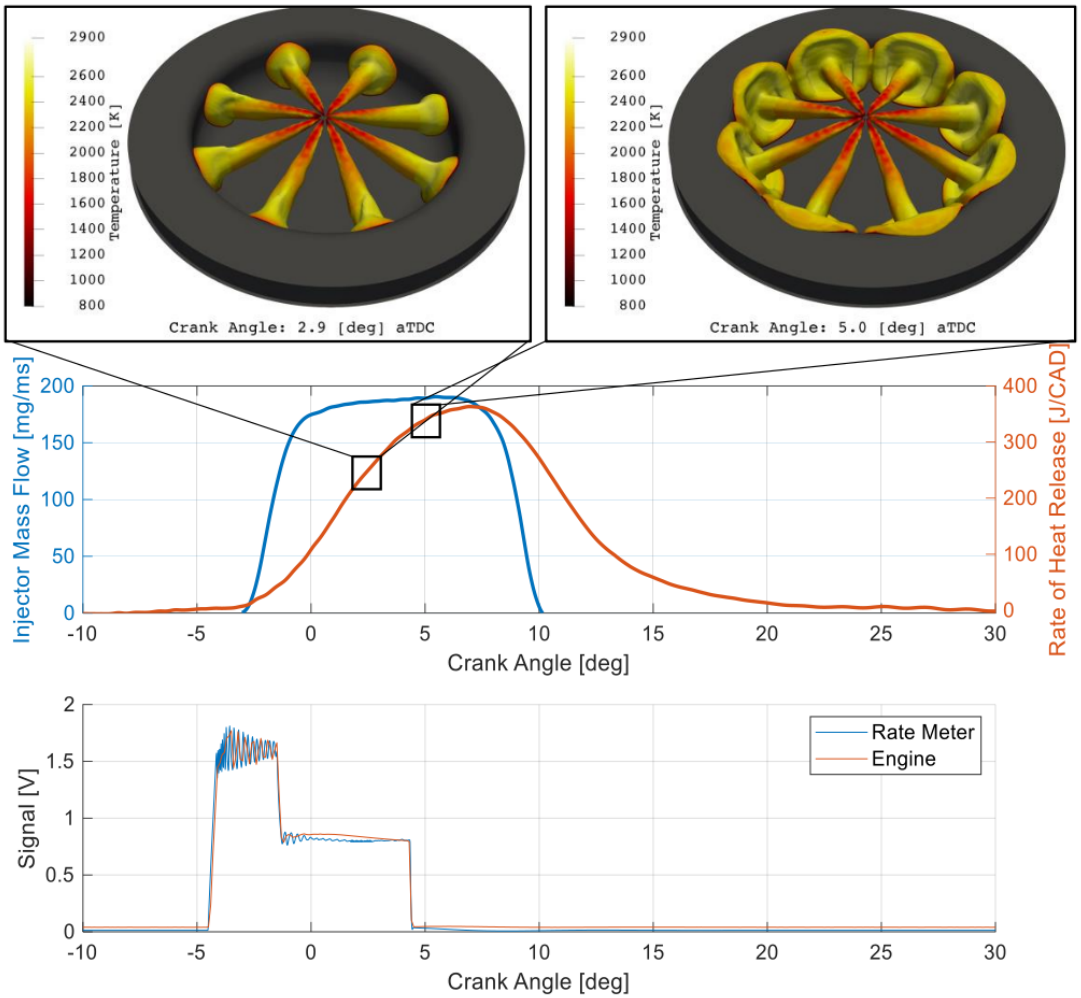

Figure 5.17: Top: CFD results showing flame-wall and flame flame interactions at 1262 RPM and 172 Nm. Middle Interpolated injection rates and aRoHR curves for methanol with an injection duration of 1172 μs. Bottom: Injector trigger signals recorded in the rate meter and the engine.

5.5 Paper 5

Paper 5 presents a CFD study of the same dual-fuel engine used in the work presented in Paper 4. This study focused only on methanol and the objectives were to validate the CFD model and study the ignition procedure. The LOGE-CPV model presented in Chapter 3 was used to model the chemistry, and the VSB2 model was used to model the spray formation of methanol and diesel.

5.5.1 Case Summary

The dual-fuel engine that was simulated was based on a Volvo D13 single-cylinder research engine with a custom cylinder head to provide mounting options for a pilot injector. The main injector was a Delphi F3 injector with an 8 hole 4.6 l/min nozzle. For the pilot fuel, a Bosch CRI-12 light duty diesel injector with a 3 hole nozzle

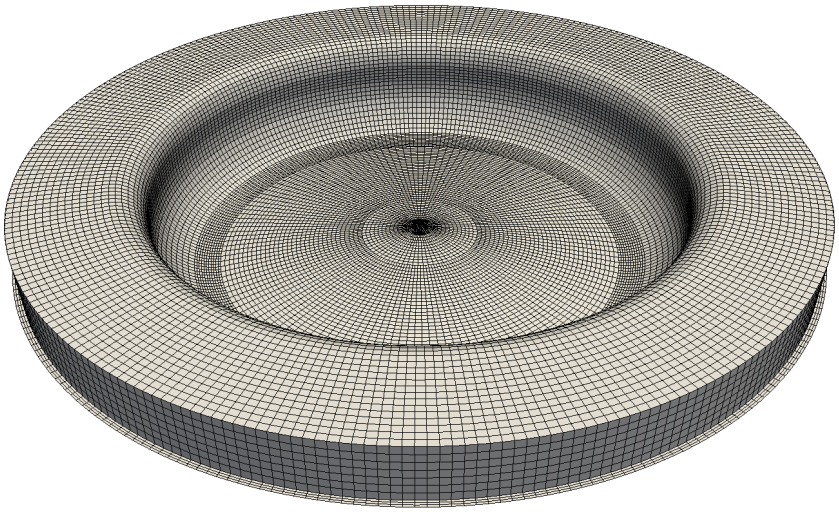

Figure 5.18: Piston bowl mesh used in the engine simulations.

positioned asymmetrically was used. The injection pressure was kept constant at 500 bar for the diesel pilot in all tests. The geometrical parameters of the engine are summarized in Table 5.5.

Table 5.5: Single Cylinder Volvo D13 Geometrical Properties.

Property	Value	Unit
Engine Displacement	2.13	l
Bore	131	mm
Stroke	158	mm
Compression Ratio	16.7:1	–

5.5.2 Numerical Setup

In all the engine simulations, only the closed part of the engine cycle was considered. This eliminated the need to model the intake and exhaust manifold. When conducting CFD modeling of a direct-injection diesel engine, sector symmetry can normally be assumed due to the center position of the injector. This symmetry was not valid in the present work due to the presence of the pilot injector. Thus, it was necessary to model the entire combustion chamber. For this purpose, a mesh consisting of 383 949 cells at TDC was used. The piston bowl mesh is shown in Figure 5.18. Due to the motion of the piston in the engine, it was necessary to implement a moving mesh procedure: the mesh motion technique known as mesh-layering from LibICE-2.2.x implemented by Politecnico di Milano was used [35]. Three different speed-load points and two EGR levels (0% and 20%) were considered. The engine operating parameters are summarized in Table 5.6 for 0 % EGR and in Table 5.7 for 20 % EGR. A proprietary multi-fuel chemical mechanism consisting of 386 species and 2343 reactions [3] was tabulated using the CPV model described in Chapter 3 and used to compute the chemical source terms.

Table 5.6: Engine initial and operating conditions for methanol cases

	Case 1	Case 2	Case 3	Unit
Torque	86	172	285	Nm
Engine Speed	873	1262	1508	RPM
SOI Main Fuel	-1.2	3.6	8.1	deg bTDC
SOI Pilot Fuel	3.9	9.6	14.7	deg bTDC
Mass of Injected Pilot Fuel	2.33	2.41	2.35	mg/stroke
Mass of Injected Main Fuel	136.71	246.41	389.90	mg/stroke
Injection Pressure Main Injector	1250	1250	1250	bar

Table 5.7: Engine initial and operating conditions for methanol cases with 20 % EGR

	Case 4	Case 5	Case 6	Unit
Torque	86	172	285	Nm
Engine Speed	871	1262	1508	RPM
SOI Main Fuel	-0.8	4.5	9.14	deg bTDC
SOI Pilot Fuel	4.3	10.5	15.8	deg bTDC
Mass of Injected Pilot Fuel	2.33	2.41	2.35	mg/stroke
Mass of Injected Main Fuel	134.55	247.41	389.90	mg/stroke
Injection Pressure Main Injector	1250	1250	1250	bar

5.5.3 Injection Rate Meter Tests

In order to accurately predict the combustion, injection rate curves were measured for the main fuel injector using methanol at different injection pressures and durations. The measurements were made using the commercially available Loccioni Mexus 2.0 system. The measured injection rates at 1250 bar are shown in Figure 5.19.

5.5.4 Pressure and Rate of Heat Release

Figure 5.20 shows the experimentally measured in-cylinder pressure and rate of heat release compared to simulated curves for a mid-load case. The predicted pressure curve showed very good agreement to the measured one with the peak pressure accurately predicted. A slight discrepancy was found in the initial pressure rise, which was amplified in the predicted rate of heat release. This indicated a faster burn rate, consistent with the limitations of the WSR approach [48, 9]. This was also reflected by a shorter tail in the simulated heat release curve. Peaks were observed in the rate of heat release curve at approximately 363 and 365 degrees, possibly due to flame-wall and flame-flame interactions, as also discussed in Paper 4. Similar observations were made when comparing low- and high-load cases to the experimental heat release and pressure curve, with good prediction of the ignition delay and peak pressure but faster burning in the simulated cases.

The effect of using EGR was also studied for all the measured speed-load points. The pressure and heat release curves for a mid-load point with 20 % EGR compared with experimental data are shown in Figure 5.21. The shapes of the heat release

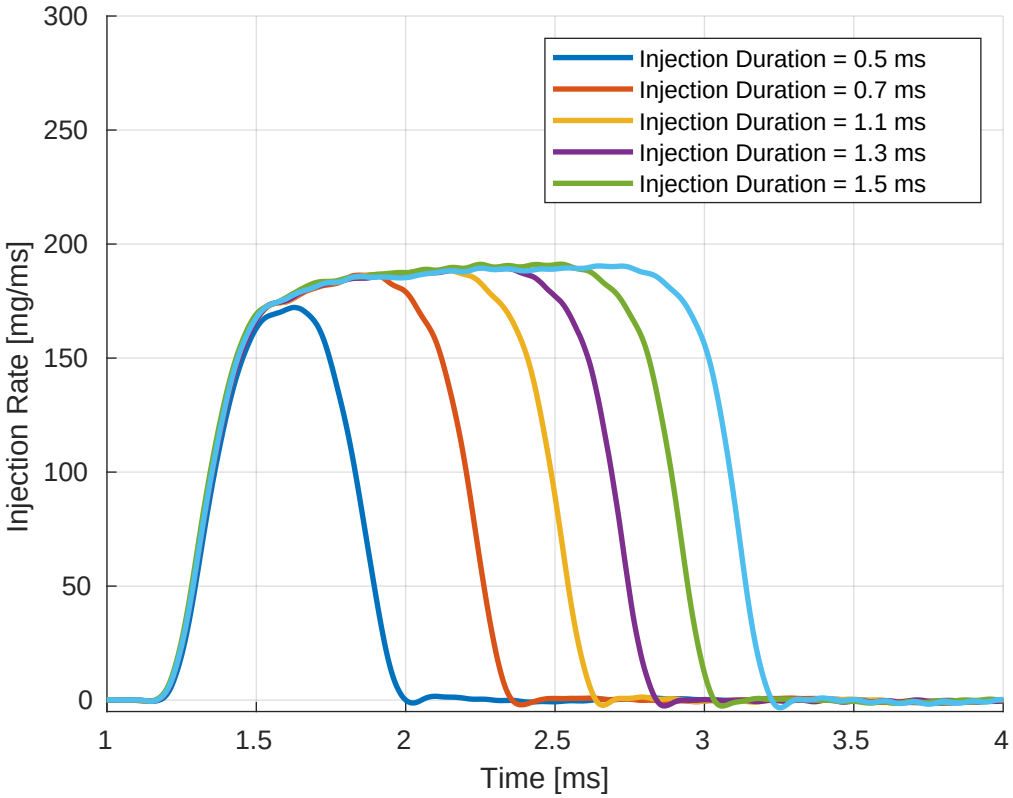

Figure 5.19: Measured injection rate at various durations for the main injector using methanol at 1250 bar injection pressure

curves were very similar to those presented in Figure 5.20. As demonstrated in Paper 4, the experimental study concluded that EGR did not seem to have any impact on the rate of heat release for methanol but had a large impact on emissions.

5.5.5 Emissions

The predicted indicated specific NO_x was compared to the measured one for all speed-load points with 0 and 20 % EGR. The results are shown in Figure 5.22. It can be seen that $ISNO_x$ is poorly predicted in almost all cases, especially those with EGR. The model predicted a reduction in $ISNO_x$ between 0 and 20 % EGR, but it was not comparable to the reduction seen in the experiments. This was likely due to the limitations of the WSR approach because the mean temperature in the reaction zone which governs thermal NOx formation tends to be higher than in models accounting for turbulence-chemistry interactions.

5.5.6 Flame Surface and Dual-Fuel Ignition

The ignition procedure in the direct-injection dual-fuel engine was studied further at the speed-load point of 1262 RPM and 172 Nm. Figure 5.23 shows a series of images of the iso-surface of the stoichiometric mixture fractions of methanol and

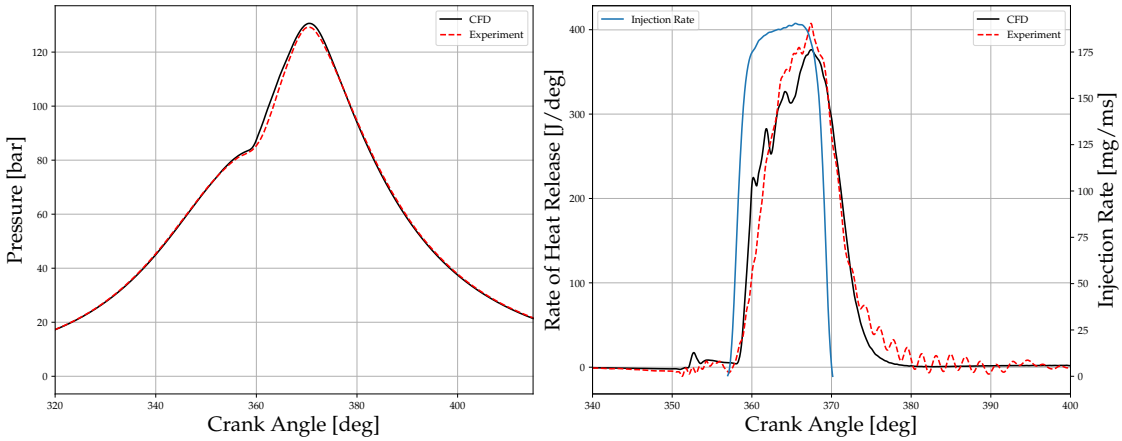

Figure 5.20: Predicted in-cylinder pressure, rate of heat release and injection rate compared to experimental values

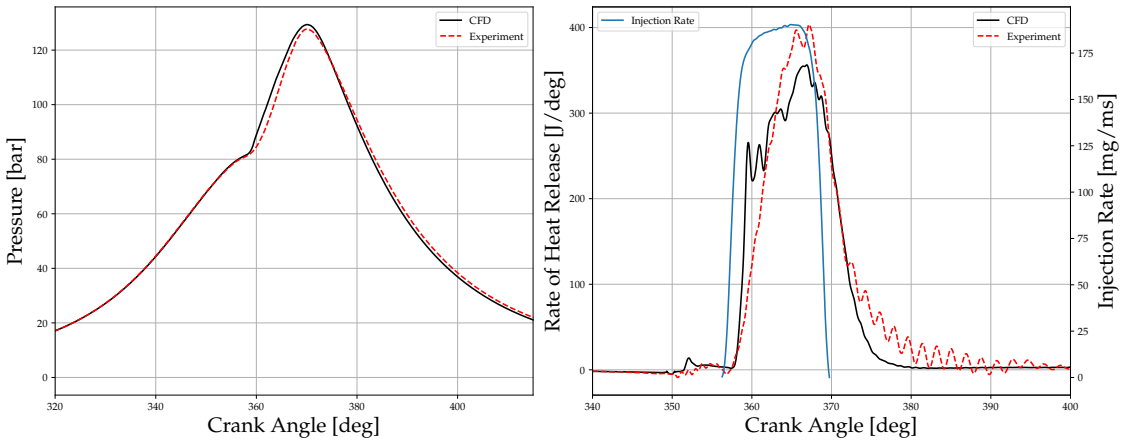

Figure 5.21: Predicted in-cylinder pressure, rate of heat release and injection rate compared to experimental values with 20 % EGR.

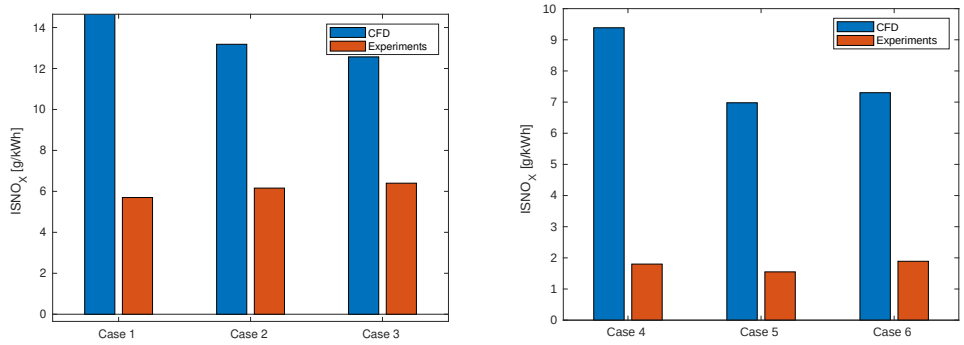

(a) No EGR (b) 20 % EGR

Figure 5.22: Comparison of measured and predicted indicated specific NO_X emissions

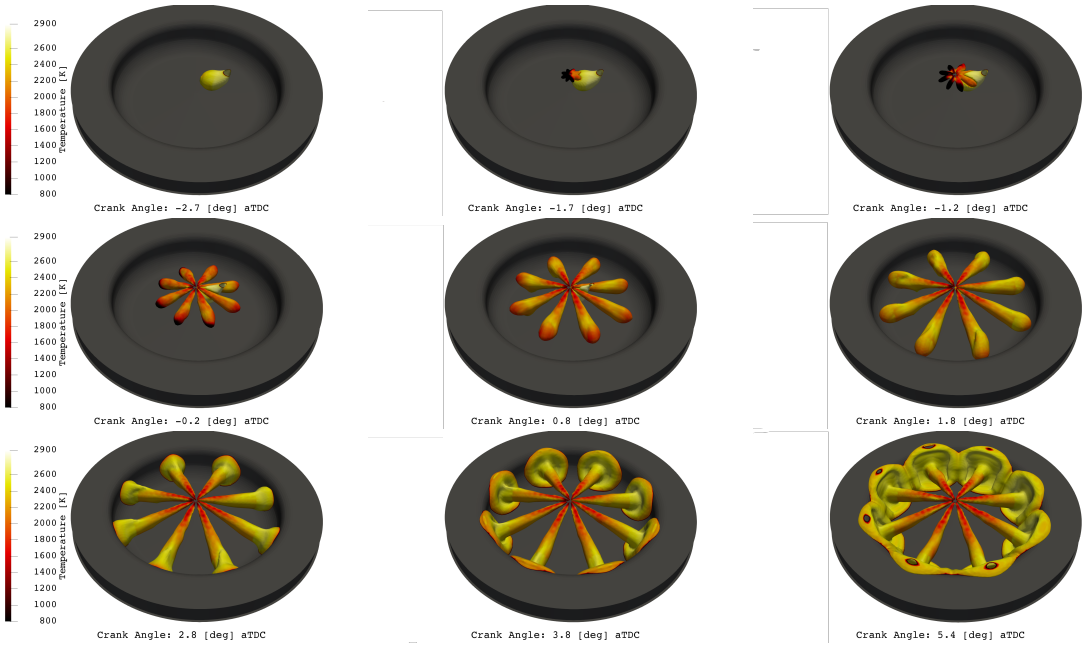

Figure 5.23: Stoichiometric surface of diesel and methanol at different crank angles colored by temperature for case 2.

diesel colored by temperature. The stoichiometric surface represents the hottest part of the flame known as the reaction zone and can be used to track the evolution of a flame in time. The pilot flame can be seen in the first picture at CAD = -2.7 deg aTDC, shortly before the main fuel was injected. It can be seen that the pilot flame was located very close to the center of the cylinder when the main fuel started to be injected. The following picture in Figure 5.23 show the stoichiometric surface just after the start of injection for methanol at CAD = -1.7 aTDC deg, Is showing that the sprays located closest to the injector are ignited first. The next picture at CAD = -1.2 deg aTDC shows that shortly after the sprays closest to the injector are ignited, there is enough heat close to the injector to ignite the remaining sprays simultaneously. In the following pictures at CAD = -0.8, 0.2 and 1.8 deg aTDC, all sprays have been fully ignited. The last three pictures at CAD = 2.8, 3.8 and 5.4 aTDC depict the flame-wall and flame-flame interactions. These results suggest that the ignition of the dual-fuel system is very stable provided there is enough heat from the pilot flame close to the methanol injector when the injection starts. This indicates that the choice of injection strategy and placement of the pilot injector in relation to the main injector are important determinants of whether the system remains stable. If the pilot flame is too far away from the methanol injector when the injection starts, the closest sprays may be ignited before the sprays opposite to the pilot injector. This would allow the methanol to mix with air for a longer time, giving the combustion a more premixed nature and making it more difficult to control.

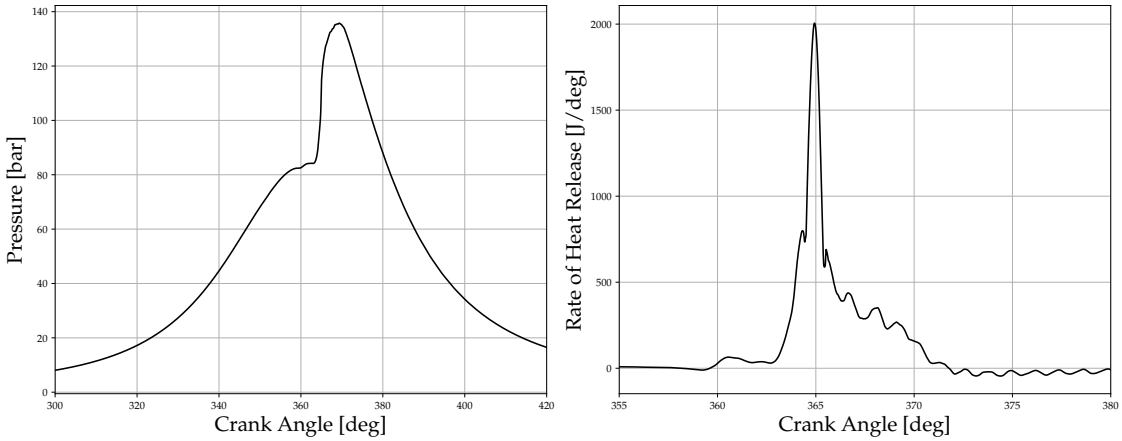

Figure 5.24: Predicted in-cylinder pressure, rate of heat release with increased pilot offset

5.5.7 Influence of Offsetting the Pilot

The influence of increasing the offset of the pilot injector relative to the main injector was also investigated. This was done to see if the stability of the ignition would be retained if the travel distance of the pilot spray to the centre would increase. The offset was increased from 22 mm to 40 mm from the centre, placing it almost at the edge of the combustion chamber. Figure 5.24 show the pressure trace and rate of heat release for the offset pilot case at the same conditions as case 2 (172 Nm, 1262 RPM). Compared to Figure 5.20, the main fuel seem to ignite later in the offset pilot case. Furthermore, a large peak can be seen in the early stages of the rate of heat release, suggesting that combustion occurs in a more premixed mode. Figure 5.25 show the ignition process in the offset pilot case in a similar manner to Figure 5.23. The first image at CAD = -1 deg aTDC show that the pilot flame has not yet reached the center of the combustion chamber when the main fuel starts to inject. At CAD = 1 deg aTDC, the two sprays closest to the pilot has ignited, but the remaining ones are not yet burning. At CAD = 3 deg aTDC, all sprays have reached the wall but only two are burning. At CAD = 5 deg aTDC all sprays are ignited, which also corresponds to the large peak in the rate of heat release seen in Figure 5.24. This suggests that the placement of the pilot injector as well as the injection timing is very important to retain control and stability of the combustion process.

5.5.8 Paper 5 conclusions

Paper 5 presents a comparison between CFD and experiments for a methanol-diesel direct-injection dual-fuel system. It was concluded that the WSR model could predict global parameters, such as the in-cylinder pressure and rate of heat release, very well for all the considered speed-load points with 0 or 20 % EGR. The predicted $ISCO_2$ and $ISNO_x$ were also compared with experimental data. The $ISCO_2$ was predicted well, but the model failed to accurately predict NO_x formation in almost all cases, especially in the presence of EGR. Therefore, for accurate predictions of emissions,

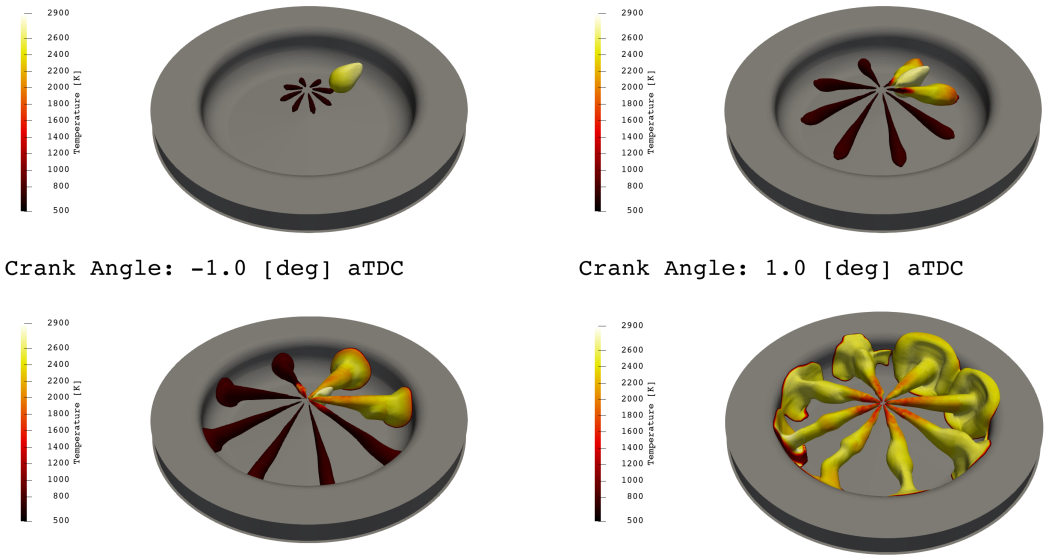

Figure 5.25: Stoichiometric surface of diesel and methanol at different crank angles colored by temperature for the offset pilot case.

a mode and regime independent turbulent combustion model should be used. The ignition process was also studied and shown to be very stable provided the hot gases from the pilot flame were in the vicinity of the main injector.

Chapter 6

Conclusions and Outlook

In Chapter 1, several research questions were set out for this thesis. Answers to these questions are discussed in this chapter. Furthermore, suggestions are made for future studies.

6.1 Conclusions and Answers to Research Questions

- **What is the influence of creating new child blobs from the stable droplets in the VSB2 spray model?** The existing breakup formulation in the VSB2 model was extended and the impact of creating child blobs was studied. It was concluded that the improved breakup treatment yielded better predictions of spray penetration at the low temperature case at 700 K, whereas in the high temperature case at 900 K it had virtually no impact. At high temperatures, there is enough energy available for evaporation that creating new blobs with stable droplets does not affect the rate of evaporation or liquid penetration.

- **Is it possible to model the formation of an alcohol spray using the VSB2 spray model without any conceptual changes to the model?** The model was originally formulated with diesel sprays in mind. It was concluded that the model could accurately predict the penetration of an alcohol spray if the turbulence parameters were tuned appropriately and the turbulent length scale was fixed in the injector cell.

- **What does the combustion process look like inside a direct-injection dual-fuel engine?** The ignition and combustion process inside a diesel-methanol direct-injection dual-fuel engine was studied using CFD. In the engine configuration studied, the combustion process was shown to be very stable and the combustion occurred almost completely in the non-premixed mode with almost no ignition delay. The CFD studies showed that the diesel flame was located almost directly under the main injector and the methanol was injected directly into a cloud of hot gases. Increasing the distance from

the pilot injector to the main injector increased the premixed characteristics of the combustion.

- **Can we model the combustion process inside a direct-injection dual-fuel engine using a simplified model that does not account for turbulence-chemistry interactions?** Turbulence-chemistry interactions have been demonstrated in the literature to play an important role in the structure of turbulent flames. In this thesis, it was demonstrated that not accounting for turbulence chemistry interactions in a dual-fuel system can still yield good predictions of the global parameters, such as the in-cylinder pressure and rate of heat release. However, it was also found that the predictions of pollutant formation were not accurate and that a turbulent combustion model is most likely necessary for accurate prediction of the formation of these pollutants.

6.2 Outlook & Further Studies

For further studies with the VSB2 spray model, it would be interesting to further investigate the improved breakup treatment. It would be possible to expand the concept by creating child blobs from all the droplet sizes in the size distribution. It should also be investigated if 10 different size interval is optimal, as this was chosen arbitrarily. Furthermore, it would also be of interest to couple VSB2 to a primary breakup model and investigate how that affect the model. Finally, it would be interesting to propose an alternative droplet size distribution function and investigate how that affect the droplet size distribution predicted by the model.

For the engine simulations, it would be interesting to compare the WSR results presented in this thesis with results computed using a turbulent combustion model, such as the transported PDF model. The expectation is that this would greatly improve the prediction of pollutant formation. If a transported PDF model would be coupled to the tabulated chemistry approach used in this work, there is great potential to reduce the calculation time of a very computationally demanding model such as the transported PDF model. Furthermore, it would be interesting to study more parametric variations of the engine hardware, such as different nozzle sizes or piston shapes. The current hardware concept seems to run very stable, but it has not been optimized. There is potential for even greater performance if a proper engine optimization was done together with CFD.

Bibliography

[1] C. Baumgarten. *Mixture Formation in Internal Combustion Engines*. Heidelberg: Springer-Verlag, 2006 (cit. on pp. 8, 10).

[2] S. Bhattacharjee and D. C. Haworth. "Simulations of transient n-heptane and n-dodecane spray flames under engine-relevant conditions using a transported PDF method". In: *Combustion and Flame* 160.10 (2013), pp. 2083–2102. ISSN: 00102180. DOI: 10.1016/j.combustflame.2013.05.003 (cit. on pp. 10, 12).

[3] A. Borg and H. Lehtiniemi. *Fuel Flexible Engine Platform Reaction Scheme*. Confidential Report. Confidential Report, October 2017. LOGE AB (cit. on p. 42).

[4] J. Chomiak. *Combustion: A Study in Theory, Fact, and Application*. Abacus Press, 1990. ISBN: 9780856264535 (cit. on p. 11).

[5] J. Chomiak and A. Karlsson. "Flame liftoff in diesel sprays". In: *Symposium (International) on Combustion* 26.2 (1996), pp. 2557–2564. ISSN: 0082-0784. DOI: https://doi.org/10.1016/S0082-0784(96)80088-9 (cit. on p. 11).

[6] European Comission. *EU Reference Scenario 2016: Energy, Transport and GHG emissiosn, Trends to 2050*. European Union, 2016. ISBN: 978-92-79-52374-8. DOI: 10.2833/001137 (cit. on p. 3).

[7] F. Contino, H. Jeanmart, T. Lucchini, and G. D'Errico. "Coupling of in situ adaptive tabulation and dynamic adaptive chemistry: An effective method for solving combustion in engine simulations". In: *Proceedings of the Combustion Institute* 33 (Dec. 2011), pp. 3057–3064. DOI: 10.1016/j.proci.2010.08.002 (cit. on p. 11).

[8] G. D'Errico, D. Ettorre, and T. Lucchini. "Comparison of Combustion and Pollutant Emission Models for DI Diesel Engines". In: *8th International Conference on Engines for Automobiles*. Consiglio Nazionale delle Ricerche, Sept. 2007. DOI: https://doi.org/10.4271/2007-24-0045 (cit. on p. 11).

[9] G. D'Errico, T. Lucchini, F. Contino, M. Jangi, and X.-S. Bai. "Comparison of well-mixed and multiple representative interactive flamelet approaches for diesel spray combustion modelling". In: *Combustion Theory and Modelling* 18.1 (2014), pp. 65–88. DOI: 10.1080/13647830.2013.860238 (cit. on pp. 11, 43).

[10] T. Dageförde, K. Gröger, N. Kawaharada, and F. Dinkelacker. "Velocity Field Measurements with High Speed Structural Image Velocimetry in the Primary Atomization Region of Future Diesel Fuels". In: *SAE Powertrains, Fuels Lubricants Meeting*. SAE International, Sept. 2020. DOI: https://doi.org/10.4271/2020-01-2112 (cit. on p. 8).

[11] J. E. Dec. "A Conceptual Model of DI Diesel Combustion Based on Laser-Sheet Imaging*". In: *International Congress Exposition*. SAE International, Feb. 1997. DOI: https://doi.org/10.4271/970873 (cit. on p. 7).

[12] M.M. El Wakil, O.A. Ueyhara, and F.S. Myers. *A Theoretical Investigation of Heating-up Period of Injected Fuel Droplets Vaporizing in Air*. NACA Report No. TN3179. 1954 (cit. on p. 23).

[13] Engine Combustion Network. https://ecn.sandia.gov/. 2018 (cit. on p. 32).

[14] J. M. Garcia-Oliver, J. M. Pastor, A. Pandal, N. Trask, E. Baldwin, and David P. Schmidt. "DIESEL SPRAY CFD SIMULATIONS BASED ON THE $\Sigma - Y$; EULERIAN ATOMIZATION MODEL". In: *Atomization and Sprays* 23.1 (2013), pp. 71–95. ISSN: 1044-5110 (cit. on p. 29).

[15] N. Giramondi, M. Mihaescu, A. Christiansen Erlandsson, and A. Jäger. "CFD-Driven Preliminary Investigation of Ethanol-Diesel Diffusive Combustion in Heavy-Duty Engines". In: *SAE Technical Papers*. 2018-01-2192. 2018-01-2192. DOI: 10.4271/2019-01-2192 (cit. on p. 8).

[16] C.W Hirt and B.D Nichols. "Volume of fluid (VOF) method for the dynamics of free boundaries". In: *Journal of Computational Physics* 39.1 (1981), pp. 201–225. ISSN: 0021-9991. DOI: https://doi.org/10.1016/0021-9991(81)90145-5 (cit. on p. 9).

[17] T. Husberg, I. Denbratt, and A. Karlsson. "Analysis of Advanced Multiple Injection Strategies in a Heavy-Duty Diesel Engine Using Optical Measurements and CFD-Simulations ". In: *SAE Technical Paper 2008-01-1328* (2008) (cit. on pp. 10, 19).

[18] Internation Energy Agency (IEA). *CO2 emissions from heavy-duty vehicles in the Sustainable Development Scenario, 2000-2030*. https://www.iea.org/data-and-statistics/charts/co2-emissions-from-heavy-duty-vehicles-in-the-sustainable-development-scenario-2000-2030. Accessed: 2020-12-02 (cit. on pp. 3, 4).

[19] Internation Energy Agency (IEA). *Sustainable Development Scenario*. https://www.iea.org/reports/world-energy-model/sustainable-development-scenario. Accessed: 2020-12-02 (cit. on p. 3).

[20] M. Ishii and K. Mishima. "Two-fluid model and hydrodynamic constitutive relations". In: *Nuclear Engineering and Design* 82.2 (1984), pp. 107–126. ISSN: 0029-5493. DOI: https://doi.org/10.1016/0029-5493(84)90207-3 (cit. on p. 9).

[21] V. Iyer and J. Abraham. "Two-fluid modeling of spray penetration and dispersion under diesel engine conditions". In: *Atomization and Sprays* 15.3 (2005), pp. 249–269. DOI: 10.1615/atomizspr.v15.i3.10 (cit. on p. 10).

[22] M. Jangi, G. D'Errico, X.-S. Bai, and T. Lucchini. "Numerical simulation of the ECN spray a using multidimensional chemistry coordinate mapping: N-dodecane diesel combustion". In: *SAE Technical Papers* 9 (2012). DOI: 10.4271/2012-01-1660 (cit. on p. 10).

[23] M. Kampa and E. Castanas. "Human health effects of air pollution". In: *Environmental Pollution* 151.2 (2008), pp. 362–367. DOI: 10.1016/j.envpol.2007.06.012 (cit. on p. 3).

[24] A. Karlsson. "Modeling Auto-Ignition, Flame Propagation and Combustion in Non-Stationary Turbulent Sprays". PhD thesis. Chalmers University of Technology, 1995 (cit. on p. 23).

[25] F. P. Kärrholm, F. Tao, and P.N. Nordin. "Three-Dimensional Simulation of Diesel Spray Ignition and Flame Lift-Off Using OpenFOAM and KIVA-3V CFD Codes." In: *SAE paper 2008-01-0961* 2008.724 (2008), pp. 776–790. DOI: 10.4271/2008-01-0961 (cit. on p. 10).

[26] A. R. Kerstein. "A Linear-Eddy Model of Turbulent Scalar Transport and Mixing". In: *Combustion Science and Technology* 60.4-6 (1988), pp. 391–421. ISSN: 1563521X. DOI: 10.1080/00102208808923995 (cit. on p. 12).

[27] S. L. Kokjohn, R. M. Hanson, D. A. Splitter, and R. D. Reitz. *Experiments and Modeling of Dual-Fuel HCCI and PCCI Combustion Using In-Cylinder Fuel Blending*. Nov. 2009. DOI: https://doi.org/10.4271/2009-01-2647 (cit. on p. 7).

[28] A. Kösters and A. Karlsson. "Modeling of Diesel Fuel Spray Formation in OpenFOAM". In: (2011). SAE Technical Paper 2011-01-0842 (cit. on pp. 19, 29).

[29] A. Kösters and A. Karlsson. "VALIDATION OF THE VSB2 SPRAY MODEL AGAINST SPRAY A AND SPRAY H". In: *Atomization and Sprays* 26.8 (2016), pp. 775–798 (cit. on p. 19).

[30] T. Lackmann, A. R. Kerstein, and M. Oevermann. "A representative linear eddy model for simulating spray combustion in engines (RILEM)". In: *Combustion and Flame* 193 (2018), pp. 1–15. ISSN: 0010-2180. DOI: https://doi.org/10.1016/j.combustflame.2018.02.008 (cit. on p. 12).

[31] B.E. Launder and D.B. Spalding. "The numerical computation of turbulent flows". In: *Computer Methods in Applied Mechanics and Engineering* 3.2 (1974), pp. 269–289. ISSN: 0045-7825. DOI: https://doi.org/10.1016/0045-7825(74)90029-2 (cit. on p. 15).

[32] F. Li, C.F. Lee, Ziman W., H. Wu, and G. Lu. "Schlieren investigation on impacts of duct size on macroscopic spray characteristics of ducted fuel injection". In: *Applied Thermal Engineering* 176.November 2019 (2020), p. 115440. ISSN: 13594311. DOI: 10.1016/j.applthermaleng.2020.115440 (cit. on p. 8).

[33] M. Linne, M. Paciaroni, and T. Hall T.and Parker. "Ballistic imaging of the near field in a diesel spray". In: *Experiments in Fluids* 40.6 (2006), pp. 836–846. ISSN: 07234864. DOI: 10.1007/s00348-006-0122-0 (cit. on p. 8).

[34] LOGE. https://logesoft.com/loge-software/. 2020 (cit. on p. 16).

[35] T. Lucchini, G. D'Errico, H. Jasak, and Ž Tuković. "Automatic Mesh Motion with Topological Changes for Engine Simulation". In: *SAE Paper* 2007.724 (2007), pp. 01–0170. DOI: 10.4271/2007-01-0170 (cit. on p. 42).

[36] A. Maghbouli, T. Lucchini, G. D'Errico, A. Onorati, L.-M. Malbec, M.P. Musculus, and W.E. Eagle. "Parametric Comparison of Well-Mixed and Flamelet n-dodecane Spray Combustion with Engine Experiments at Well Controlled Boundary Conditions". In: *SAE Technical Papers* (2016). DOI: 10.4271/2016-01-0577 (cit. on p. 10).

[37] A. Matrisciano, T. Franken, C. Perlman, A. Borg, H. Lehtiniemi, and F. Mauss. "Development of a Computationally Efficient Progress Variable Approach for a Direct Injection Stochastic Reactor Model". In: *WCX™ 17: SAE World Congress Experience*. SAE International, Mar. 2017. DOI: https://doi.org/10.4271/2017-01-0512 (cit. on p. 16).

[38] A. Matrisciano, C. Netzer, A. Werner, A. Borg, Lars S., and F. Mauss. "A Computationally Efficient Progress Variable Approach for In-Cylinder Combustion and Emissions Simulations". In: *14th International Conference on Engines Vehicles*. SAE International, Sept. 2019. DOI: https://doi.org/10.4271/2019-24-0011 (cit. on pp. 16, 17).

[39] M. Noussan, M. Hafner, and S. Tagliapietra. *The Future of Transport Between Digitalization and Decarbonization*. Springer, 2020. ISBN: 978-3-030-37965-0. DOI: 10.1007/978-3-030-37966-7 (cit. on p. 3).

[40] P. J. O'Rourke and A.A. Amsden. "The Tab Method for Numerical Calculation of Spray Droplet Breakup". In: *1987 SAE International Fall Fuels and Lubricants Meeting and Exhibition*. SAE International, Nov. 1987. DOI: https://doi.org/10.4271/872089 (cit. on p. 10).

[41] N. Ochiai, J. Ishimoto, A. Arioka, N. Yamaguchi, Y. Sasaki, and N. Furukawa. "Integrated Computational Study for Total Atomization Process of Primary Breakup to Spray Droplet Formation in Injector Nozzle". In: *SAE 2016 International Powertrains, Fuels Lubricants Meeting*. SAE International, Oct. 2016. DOI: https://doi.org/10.4271/2016-01-2202 (cit. on p. 9).

[42] M. A. Patterson and R.D. Reitz. "Modeling the Effects of Fuel Spray Characteristics on Diesel Engine Combustion and Emission". In: *International Congress Exposition*. SAE International, Feb. 1998. DOI: https://doi.org/10.4271/980131 (cit. on p. 10).

[43] N. Peters. "Laminar diffusion flamelet models in non-premixed turbulent combustion". In: *Progress in Energy and Combustion Science* 10.3 (1984), pp. 319–339. ISSN: 0360-1285. DOI: https://doi.org/10.1016/0360-1285(84)90114-X (cit. on p. 11).

[44] M. Pilch and C.A. Erdman. "Use of breakup time data and velocity history data to predict the maximum size of stable fragments for acceleration-induced breakup of a liquid drop". In: *International Journal of Multiphase Flow* 13.6 (1987), pp. 741–757. DOI: 10.1016/0301-9322(87)90063-2 (cit. on pp. 10, 20, 21).

[45] H. Pitsch, M. Chen, and N. Peters. "Unsteady flamelet modeling of turbulent hydrogen-air diffusion flames". In: *Symposium (International) on Combustion* 27.1 (1998). Twenty-Seventh Sysposium (International) on Combustion Volume One, pp. 1057–1064. ISSN: 0082-0784. DOI: https://doi.org/10.1016/S0082-0784(98)80506-7 (cit. on p. 11).

[46] S.B. Pope. "PDF methods for turbulent reactive flows". In: *Progress in Energy and Combustion Science* 11.2 (Jan. 1985), pp. 119–192. ISSN: 03601285. DOI: 10.1016/0360-1285(85)90002-4 (cit. on p. 12).

[47] Wolfgang R. *Turbulence models and their application in hydraulics: A state-of-the-art review, third edition*. Nov. 2017, pp. 1–108. ISBN: 9780203734896. DOI: 10.1201/9780203734896 (cit. on p. 28).

[48] V. Raj Mohan and D. C. Haworth. "Turbulence-chemistry interactions in a heavy-duty compression-ignition engine". In: *Proceedings of the Combustion Institute* 35.3 (2015), pp. 3053–3060. ISSN: 15407489. DOI: 10.1016/j.proci.2014.06.098 (cit. on pp. 10, 12, 43).

[49] W.E. Ranz and W.R. Marshall. "Evaporation from Drops". In: *Chem. Eng. Prog* 48.3 (1952), pp. 141–146 (cit. on p. 23).

[50] R. D. Reitz. "Modeling Atomization Processes in High-Pressure Vaporizing Sprays". In: *Atomization and Spray Technology 3*. 1987, pp. 309–337 (cit. on p. 10).

[51] R. D. Reitz and R. Diwakar. "Structure of High-Pressure Fuel Sprays". In: *SAE International Congress and Exposition*. SAE International, Feb. 1987. DOI: https://doi.org/10.4271/870598 (cit. on pp. 10, 20).

[52] R. D. Reitz and G. Duraisamy. "Review of high efficiency and clean reactivity controlled compression ignition (RCCI) combustion in internal combustion engines". In: *Progress in Energy and Combustion Science* 46 (2015), pp. 12–71. ISSN: 0360-1285. DOI: https://doi.org/10.1016/j.pecs.2014.05.003 (cit. on p. 7).

[53] R. Schmehl, G. Maier, and S. Wittig. "CFD analysis of fuel atomization, secondary droplet breakup and spray dispersion in the premix duct of a LPP combustor". In: *8th International Conference on Liquid Atomization and Spray Systems* July (2000), p. 8 (cit. on p. 23).

[54] J. Schutze, V. Kumar, R. Sonawane, M. Braun, and M. Sami. "A multi-model hybrid approach for the numerical simulation of fluid phase dispersion processes". In: *ICLASS 2018 - 14th International Conference on Liquid Atomization and Spray Systems*. July 2018 (cit. on p. 9).

[55] P. K. Senecal, E. Pomraning, K. J. Richards, T. E. Briggs, C. Y. Choi, R. M. McDavid, and M. A. Patterson. "Multi-Dimensional Modeling of Direct-Injection Diesel Spray Liquid Length and Flame Lift-off Length using CFD and Parallel Detailed Chemistry". In: *SAE 2003 World Congress Exhibition*. SAE International, Mar. 2003. DOI: https://doi.org/10.4271/2003-01-1043 (cit. on p. 11).

[56] T.H. Shih, W. W. Liou, A. Shabbir, Z. Yang, and J. Zhu. "A new k- eddy viscosity model for high reynolds number turbulent flows". In: *Computers Fluids* 24.3 (1995), pp. 227–238. ISSN: 0045-7930. DOI: https://doi.org/10.1016/0045-7930(94)00032-T (cit. on p. 31).

[57] K. Sone and S. Menon. "Effect of Subgrid Modeling on the In-Cylinder Unsteady Mixing Process in a Direct Injection Engine". In: *Journal of Engineering for Gas Turbines and Power-transactions of The Asme - J ENG GAS TURB POWER-T ASME* 125 (Apr. 2003). DOI: 10.1115/1.1501918 (cit. on p. 12).

[58] S. H. E. Tahry. "k-epsilon equation for compressible reciprocating engine flows". In: *Journal of Energy* 7.4 (1983), pp. 345–353. DOI: 10.2514/3.48086 (cit. on p. 15).

[59] R. Torelli, G. D'Errico, T. Lucchini, V. Ikonomou, and R. M. McDavid. "A SPHERICAL VOLUME INTERACTION DDM APPROACH FOR DIESEL SPRAY MODELING". In: *Atomization and Sprays* 25.4 (2015), pp. 335–374. ISSN: 1044-5110 (cit. on p. 29).

[60] T.L. Ullman, C. T. Hare, and T. M. Baines. "Emissions from Direct-Injected Heavy-Duty Methanol-Fueled Engines (One Dual-Injection and One Spark-Ignited) and a Comparable Diesel Engine". In: *West Coast International Meeting and Exposition*. SAE International, Feb. 1982. DOI: https://doi.org/10.4271/820966 (cit. on p. 8).

[61] United Nations Framework Convention on Climate Change. *The Paris Agreement*. https://unfccc.int/process-and-meetings/the-paris-agreement/the-paris-agreement. Accessed: 2020-12-02 (cit. on p. 3).

[62] H.K. Versteeg and W. Malalasekera. *An Introduction to Computational Fluid Dynamics: The Finite Volume Method*. Pearson Education Ltd, 2007. ISBN: 978-0-13-127498-3 (cit. on p. 15).

[63] H. G. Weller, G. Tabor, H. Jasak, and C. Fureby. "A tensorial approach to computational continuum mechanics using object-oriented techniques". In: *Computers in Physics* 12.6 (1998), p. 620. ISSN: 08941866. DOI: 10.1063/1.168744 (cit. on p. 27).

[64] X. Yang, A. Solomon, and T.W Kuo. "Ignition and Combustion Simulations of Spray-Guided SIDI Engine using Arrhenius Combustion with Spark-Energy Deposition Model". In: *SAE 2012 World Congress Exhibition*. SAE International, Apr. 2012. DOI: https://doi.org/10.4271/2012-01-0147 (cit. on p. 11).

[65] J. Zeldovich. “The Oxidation of Nitrogen in Combustion and Explosions”. In: *Acta Physicochimica URSS* (1946) (cit. on p. 7).